In Situ Burning of Oil Spills: Mesoscale Experiments and Analysis*

William D. Walton, David D. Evans, Kevin B. McGrattan, Howard R. Baum, William H. Twilley, Daniel Madrzykowski, Anthony D. Putorti, Ronald G. Rehm
National Institute of Standards and Technology
Technology Administration
U.S. Department of Commerce
Gaithersburg, MD 20899

and

Hiroshi Koseki
Fire Research Institute
Fire Defence Agency
Ministry of Home Affairs
Mitaka, Tokyo 181, Japan

Edward J. Tennyson
Technology Assessment and
Research Branch
Minerals Management Service
U.S. Department of the Interior
Herndon, VA 22070

Proceeding of the Sixteenth Arctic and Marine Oil Spill Program
Technical Seminar
June 7-9, 1993
Calgary, Alberta

*Revised November 1, 1993

In Situ Burning of Oil Spills: Mesoscale Experiments and Analysis

William D. Walton, David D. Evans, Kevin B. McGrattan, Howard R. Baum, William H. Twilley, Daniel Madrzykowski, Anthony D. Putorti, Ronald G. Rehm
National Institute of Standards and Technology
Technology Administration
U.S. Department of Commerce
Gaithersburg, MD 20899

and

Hiroshi Koseki
Fire Research Institute
Fire Defence Agency
Ministry of Home Affairs
Mitaka, Tokyo 181, Japan

Edward J. Tennyson
Technology Assessment and Research Branch
Minerals Management Service
U.S. Department of the Interior
Herndon, VA 22070

ABSTRACT

A series of six mesoscale and one large laboratory fire experiments were performed to measure the burning characteristics of Louisiana crude oil on water in a pan. These included one - 6 m square and five - 15 m square mesoscale burns and one - 1.2 m diameter laboratory burn. Results of the measurements for burning rate and smoke emissions are compared to those from previous burns of various scales. The burning rate as indicated by the regression rate of the oil surface was found to be 0.062 ± 0.003 mm/s for both the 6 m and 15 m square pan fires and 0.046 mm/s for the 1.2 m diameter fire. Smoke particulate yields from both the 15 m square and 1.2 m diameter fires were found to be approximately 11% of the oil burned on a mass basis. Predictions of smoke plume trajectory and particulate deposition at ground level from the Large Eddy Simulation (LES) model developed as part of this research effort are presented. LES is a steady-state three-dimensional calculation of smoke plume trajectory and smoke particulate deposition based on a mixed finite difference and Lagrangian particle tracking method.

INTRODUCTION

In-situ burning of spilled oil has distinct advantages over other countermeasures. It offers the potential to convert rapidly large quantities of oil into its primary combustion products, carbon dioxide and water, with a small percentage of smoke particulate and other unburned and residue byproducts. Burning of spilled oil from the water surface reduces the chances of shoreline contamination and damage to biota by removing the oil from the water surface before it spreads and moves. In situ

burning requires minimal equipment and less labor than other techniques. It can be applied in areas where many other methods cannot due to lack of response infrastructure and/or lack of alternatives. Oil spills amongst ice and on ice are examples of situations where practical alternatives to burning are very limited. Because the oil is mainly converted to airborne products of combustion by burning, the need for physical collection, storage, and transport of recovered fluids is reduced to the few percent of the original spill volume that remains as residue after burning.

Burning oil spills produces a visible smoke plume containing smoke particulate and other products of combustion which may persist over many kilometers downwind from the burn. This fact gives rise to public health concerns, related to the chemical content of the smoke plume and the downwind deposition of particulate, which need to be answered. Air quality is also affected by evaporation of large oil spills that are not burned. Volatile organic compounds (VOC) including benzene, toluene, and xylene and polycyclic aromatic hydrocarbons (PAH) are found in the air downwind of an evaporating crude oil spill. Laboratory measurements are useful to determine the types of chemical compounds that can be expected from large oil spill burns or the evaporation of the spill. To determine the rate of emissions and the transport of the chemical compounds from a burning or evaporating spill, mesoscale experiments have been conducted outdoors using a 15 m square pan. In these experiments a layer of crude oil was discharged onto the surface of a salt water pool and burned.

BACKGROUND

Extensive experimental studies to quantify the capabilities of in situ burning began in 1983 at the Oil and Hazardous Materials Simulated Environmental Test Tank (OHMSETT) facility in Leonardo, New Jersey under joint funding from the Minerals Management Service (MMS), U.S. Coast Guard (USCG), Environmental Protection Agency (EPA), and Environment Canada (EC). Results showed that 50 to 95 percent of all of the oils tested could be removed from the water surface by burning [1-4].

Based upon the success of these research efforts, a joint MMS and EC in situ burning research program continued in 1985. This research program was designed to study how burning large oil spills would affect air quality by quantifying the products of combustion and developing methods to predict the downwind smoke particulate deposition. Initially, laboratory experiments were conducted by the Center for Fire Research, now the Building and Fire Research Laboratory, at the National Institute of Standards and Technology (NIST) [5-8]. This work sought to quantify the processes involved in oil spill combustion on water and included measurements of smoke production and prediction of smoke dispersal. Technical support from EC allowed the study to be broadened to include chemical analysis of the oil, oil residue, and oil smoke.

Mesoscale outdoor burns were conducted to verify that the favorable results obtained in the laboratory would apply to burns at a scale approaching that expected to be used in oil spill mitigation. New instrumentation techniques were developed to conduct measurements during the mesoscale burns and have been improved and refined in subsequent mesoscale and large indoor burns [9-13].

During this same time period, development continued on the Large Eddy Simulation (LES) model for the calculation of smoke plume trajectory and predicting the "footprint" of soot particle deposition downwind of a burn. LES is a steady-state three-dimensional calculation of smoke plume trajectory and smoke particulate deposition based on a mixed finite difference and Lagrangian particle tracking method[13].

EXPERIMENTAL FACILITIES

To understand the important features of in situ burning it is necessary to perform both laboratory and mesoscale experiments. In addition, burns of intentional releases of crude oil at sea at the scale of an anticipated response will be necessary to measure the effects of increased burn area, waves, and movement of oil over the water in a boom, which have not been assessed in laboratory and mesoscale experiments. In this research program there is a continuing interaction between findings from measurements on small fire experiments performed in the controlled laboratory environments of NIST and the Fire Research Institute (FRI) in Japan, and large fire experiments at facilities such as the USCG Fire Safety and Test Detachment in Mobile, Alabama where outdoor mesoscale liquid fuel burns in large pans are possible.

Through the cooperation of the Fire Research Institute (FRI) in Tokyo, Japan, joint studies of crude oil burning characteristics were conducted. FRI maintains a 24 m × 24 m × 20 m high fire test facility in which crude oil pools up to 3 m in diameter can be burned, with all of the combustion products collected in a large hood system. This facility could accommodate fires that are large enough so that sampling packages designed for mesoscale tests could be evaluated.

MESOSCALE CONFIGURATION

The mesoscale burns of crude oil were carried out under the direction of NIST at the United States Coast Guard Fire and Safety Test Detachment facility on Little Sand Island in Mobile Bay, Alabama. Little Sand Island is approximately 0.2 km^2 in size and includes three decommissioned ships docked in a lagoon. The ships and facilities on the island have been used for a wide variety of full-scale marine fire tests. Figure 1 is a photograph of a burn in progress, and figure 2 is a plan view of the portion of the island used for the mesoscale oil spill burns.

The burns were conducted in a nominal 15 m square steel burn pan constructed specifically for oil spill burning. The burn pan was 0.61 m deep and was constructed with two perimeter walls approximately 1.2 m apart forming an inner and outer area of the pan. The inside dimensions of the inner area of the pan were 15.2 m by 15.2 m. The two perimeter walls were connected with baffles and the space between the walls, which formed the outer area of the pan, was filled with bay water during the burns. The base of the pan was 6 mm thick steel plate and the walls were 5 mm thick steel plate. The tops of the walls were reinforced with steel angle to prevent warping during the burns. The base of the pan was located on ground level and was reinforced with steel beams on steel footers under the pan. Water fill pipes were connected to both the inner and outer areas of the pan. Water was pumped directly

Figure 1. 15.2 m square mesoscale crude oil burn

from Mobile Bay into both the inner and outer areas of the pan. The inner area of the pan was filled with approximately 0.5 m of water and the crude oil was added on top of the water. A sand oil spill containment dike approximately 0.5 m high was constructed around the perimeter of the pan 4 m from the outer edge.

The crude oil used in the mesoscale burns was obtained from an oil storage facility in Louisiana. The oil originated from wells in the Louisiana area and is thus referred to as Louisiana crude oil. The oil was 85.79% carbon, 13.25% hydrogen, and 0.41% sulfur by mass as measured by a commercial testing laboratory.

Crude oil was pumped to the burn pan via an underground pipe. A vertical section of the oil fill pipe penetrated the base of the pan and terminated in a fitting to disperse the oil horizontally below the water level. The supply side of the oil fill pipe terminated approximately 200 m from the burn pan. Gate valves were located in the supply pipe next to the pan, 52 m from the pan and at the supply point. A check valve and a orifice plate flow meter were located in the supply pipe near the pan.

Two different primary burn areas were used in the series. These areas consisted of the full inner pan with an area of 231 m^2 and a partial pan area of 37.2 m^2. The partial pan area was achieved by partitioning a corner of the inner pan with two 6.1 m sections of fire resistant boom.

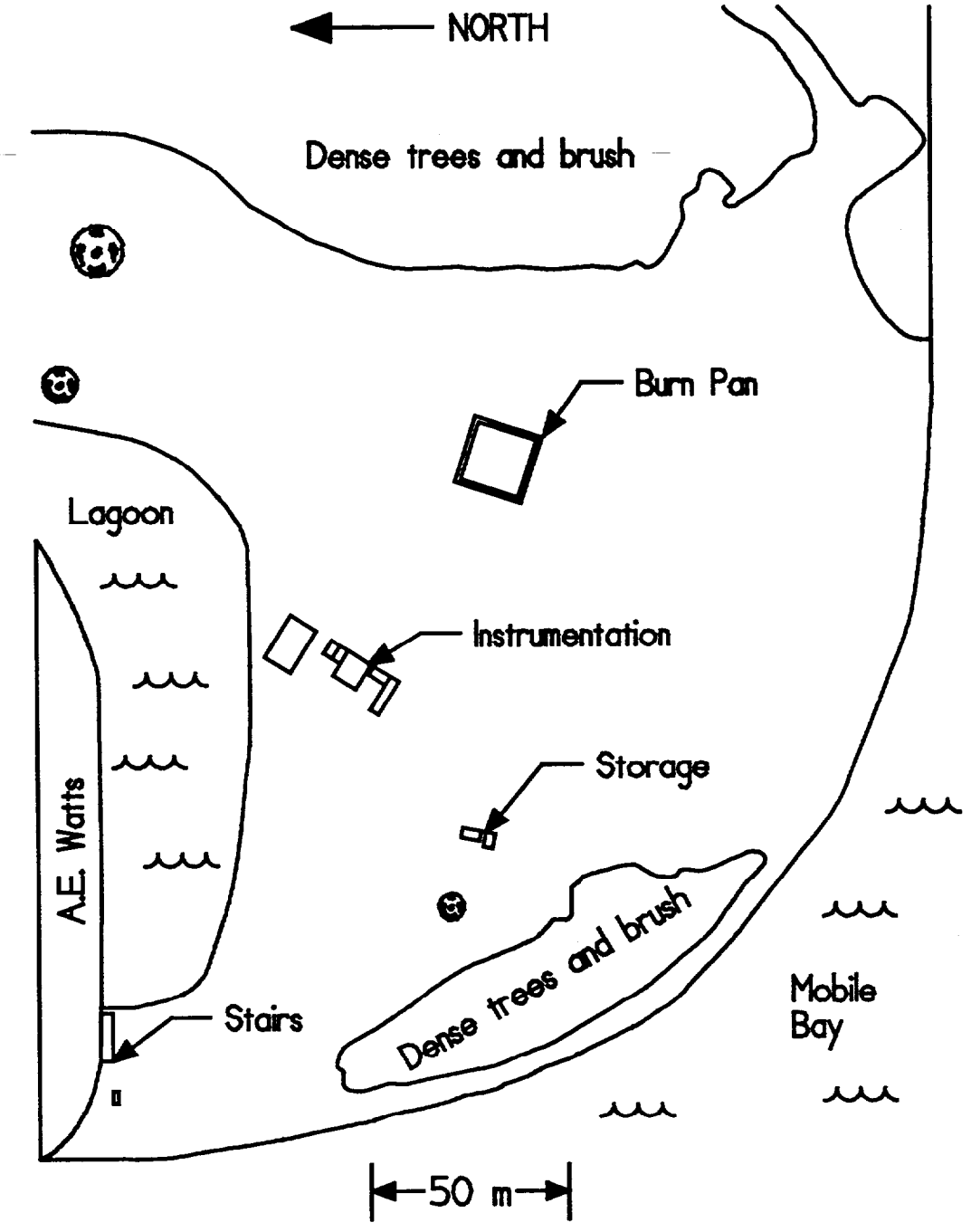

Figure 2. USCG mesoscale burn facility site plan

A total of 6 mesoscale burns were conducted. Table 1 gives the size and areas for the mesoscale burns. An effective diameter was calculated for both of the rectangular burn areas. The effective diameter is the diameter of a circle with the same area as the rectangular burn area used.

Table 1. Mesoscale burn size

Burn No.	Burn Size (m)	Burn Area		Effective Burn Diameter		Burn Area/ Full Pan Area (%)	Features
		(m^2)	(ft^2)	(m)	(ft)		
1103	6.10 × 6.10	37.2	400	6.88	22.6	16	boom formed two sides of burn area
1105	15.2 × 15.2	231	2490	17.2	56.4	100	
1106	15.2 × 15.2	231	2490	17.2	56.4	100	
1107	15.2 × 15.2	231	2490	17.2	56.4	100	
1109	15.2 × 15.2	231	2490	17.2	56.4	100	
1110	15.2 × 15.2	231	2490	17.2	56.4	100	

LABORATORY CONFIGURATION

The laboratory burn of crude oil was carried out jointly under the direction of the Fire Research Institute (FRI) in Tokyo, Japan and NIST at the FRI fire test facility. The facility consists of a 24 m x 24 m x 20 m high indoor burn hall, where all of the combustion products are collected into a smoke scrubbing exhaust system from inlets near the ceiling. The single crude oil burn was carried out in a 1.2 m diameter, 0.33 m deep steel pan placed on 25 mm thick insulating board on the floor in the center of the burn area as shown in figure 3.

MESOSCALE INSTRUMENTATION

The fixed position instrumentation in the burn pan consisted of a manometer and pressure transducer to measure the liquid level in the pan. Since the oil and the water in the pan had different densities, a correction was applied to determine the thickness of the oil layer during the burn. A copper tube was connected to the inner pan through a pipe penetrating the inner and outer walls of the pan. The tube ran underground to the instrumentation building and connected to a liquid manometer and a pressure transducer. The output from the pressure transducer was recorded every two seconds on a computerized data acquisition system.

A portable array of 8 - 0.5 mm diameter bare-bead thermocouples 76 mm apart was used to determine the temperature of the water in the inner pan at two locations on opposite sides of the pan before and after the burns.

Measurements of atmospheric conditions were made with two ground based and one airborne weather stations. The first ground based station was located 58 m at 255° from the southwest corner of the burn pan and 2.1 m above the ground. The second ground based weather station was located 49 m at 240° from the southwest corner of the burn pan and 2.6 m above the ground. Both ground stations consisted of a

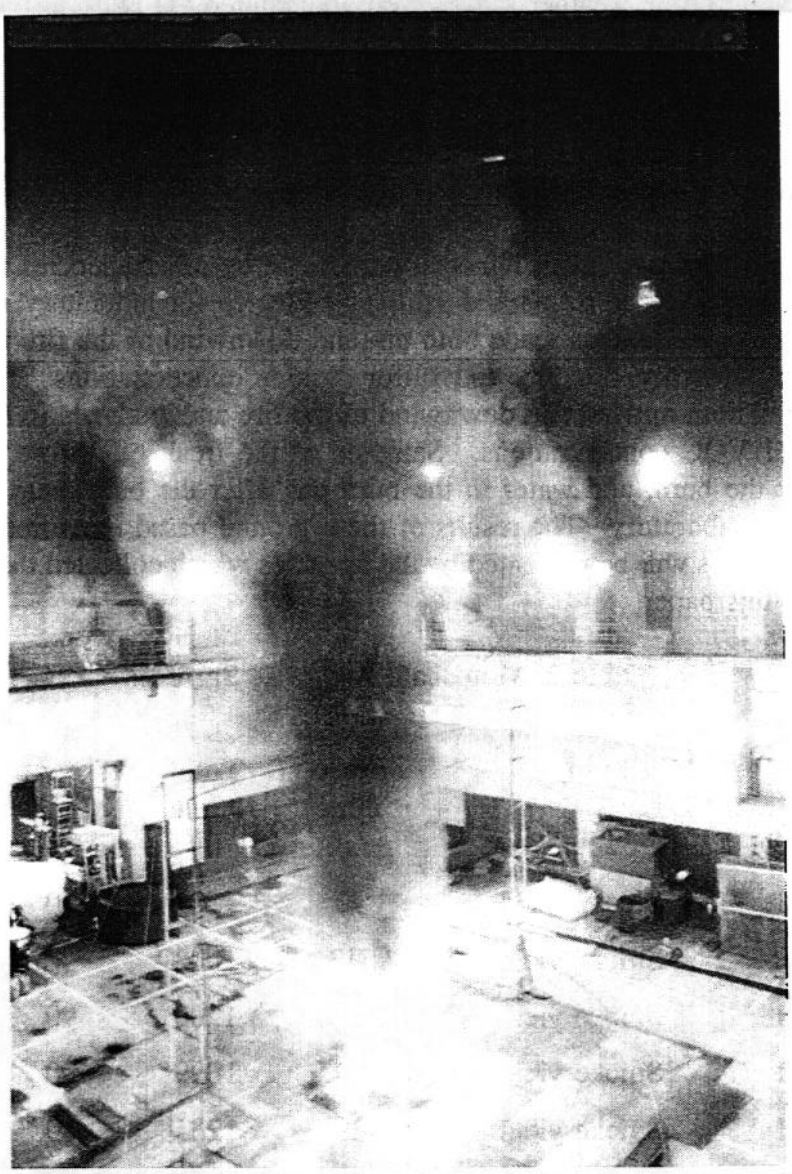

Figure 3. 1.2 m diameter crude oil laboratory burn at FRI

thermistor to measure temperature, a propeller on vane anemometer to measure wind direction and speed, and a capacitive relative humidity sensor. In addition the first weather station had a silicon photodiode pyranometer to measure incident solar radiation. Atmospheric data from the first ground based weather station were recorded every 30 s and from the second station every 32 s with a computerized data acquisition system. The airborne weather station was connected to a helium filled miniblimp which was tethered approximately 30 m above the ground and located approximately 50 m from the pan upwind of the fire and well away from the effects of the fire plume. The airborne weather station consisted of a thermistor to measure temperature, a cup anemometer to measure wind speed, an electronic compass to measure wind direction, and a pressure transducer to measure barometric pressure.

Data from the airborne weather station were transmitted via radio to a ground based computerized data collection system every 20 s.

The ground based measurements consisted of gas samples which were collected at regular intervals both up- and downwind of the fire. These samples were analyzed for carbon dioxide concentration on site after the burn.

Additional ground based measurements were made by other agencies and consisted of both real time measurements and samples collected for laboratory measurement. The real time measurements made both up- and downwind of the fire included total particulates and carbon dioxide, and sulfur dioxide concentrations. Filter samples were collected both upwind and downwind of the fire and analyzed in the laboratory for PAH and VOC concentrations. Samples of the fresh oil before the burn, oil residue after the burn, and water in the burn pan after the burn were collected for analysis in the laboratory. The results of these ground based measurements and the laboratory analysis will be presented by the agencies which collected the data and are not given in this paper.

Table 2. Mesoscale Airborne Samples

Burn No.	Miniblimp No.	Sample	Start Time (s)	Total Time (s)	Range (m)	Altitude (m)
1103	1	Smoke yield	92	1227	70	30
	2	Smoke yield	317	1002		
1105	1	Smoke yield	60	1200	90	90
1106	1	Smoke yield	50	1099	90	80
1107	1	Smoke yield	23	1235	80	140
	2	Smoke yield	23	1235		
1109	1	Smoke yield	49	1050	40	220
	2	Smoke yield	49	1050		
	3	Smoke yield	609	490		
1110	1	Smoke yield	41	1508	80	110
	2	Smoke yield	41	1508		
	3	Impactor	41	1508		

Note: All times from ignition

Airborne samples were collected for both laboratory analysis and analysis on the ground immediately following the burns. Table 2 gives a list of the airborne samples taken. The sampling packages were suspended approximately 60 m below a 9.0 m

long 3.3 m diameter tethered helium filled miniblimp. The miniblimp was positioned downwind from the fire with the sampling package centered in the smoke plume. The elevation and downwind position of the sampling package varied with each burn as a function of the plume position. Typically, sampling packages remained in the plume for over 1000 seconds which permitted an adequate sample to be collected and allowed the natural fluctuations in the plume to be averaged. Since the lift capacity of the miniblimp was limited, depending on the elevation of the plume anticipated prior to the burn, from 1 to 4 sampling packages were deployed at a time.

LABORATORY INSTRUMENTATION

The fixed instrumentation in the burn pan consisted of a manometer and pressure transducer to measure the liquid level in the pan. A pipe which penetrated the wall of the pan was connected to a liquid manometer and a pressure transducer. The output from the pressure transducer was recorded on a chart recorder and digitized manually after the burn.

A sampling array consisting of three stations spaced one meter apart was constructed at NIST, for use in the laboratory experiment at FRI in Japan. Each of the three sampling stations consisted of three battery powered pumps. Two of these pumps drew samples through a filter and discharged a portion of the gas into a collection bag. The third pump drew a sample through a cascade impactor. Figure 4 shows one of the three identical sampling stations used in the laboratory experiment. The sampling packages were suspended approximately 15 m above the fuel surface on a cable anchored to the sides of the building as shown in figure 5. The cable extended horizontally across the centerline of the pan. The sampling packages were located on the plume axis, and along the cable at radial distances of 1 and 2 m from the plume axis. Filter samples were weighed in the laboratory and gas samples analyzed for carbon dioxide concentration using a gas chromatograph. The smoke yield was determined from these measurements. Particulate size distribution was determined by weighing the collection substrate in each stage of the cascade impactor. One of the smoke yield packages at the centerline position malfunctioned during the burn.

MESOSCALE BURN PROCEDURE

Prior to pumping crude oil into the pan, water was pumped into the outer pan so that the water level was nearly to the top of the pan. Water was also pumped into the inner pan so that the water surface level was approximately 110 mm below the top of the pan. The distance from four reference points at the top of each side of the pan to the surface of the water in the inner pan was measured and recorded. The temperature profile of the water in the inner pan was measured at two locations on opposite sides of the pan. A water sample from the inner pan was analyzed for salinity.

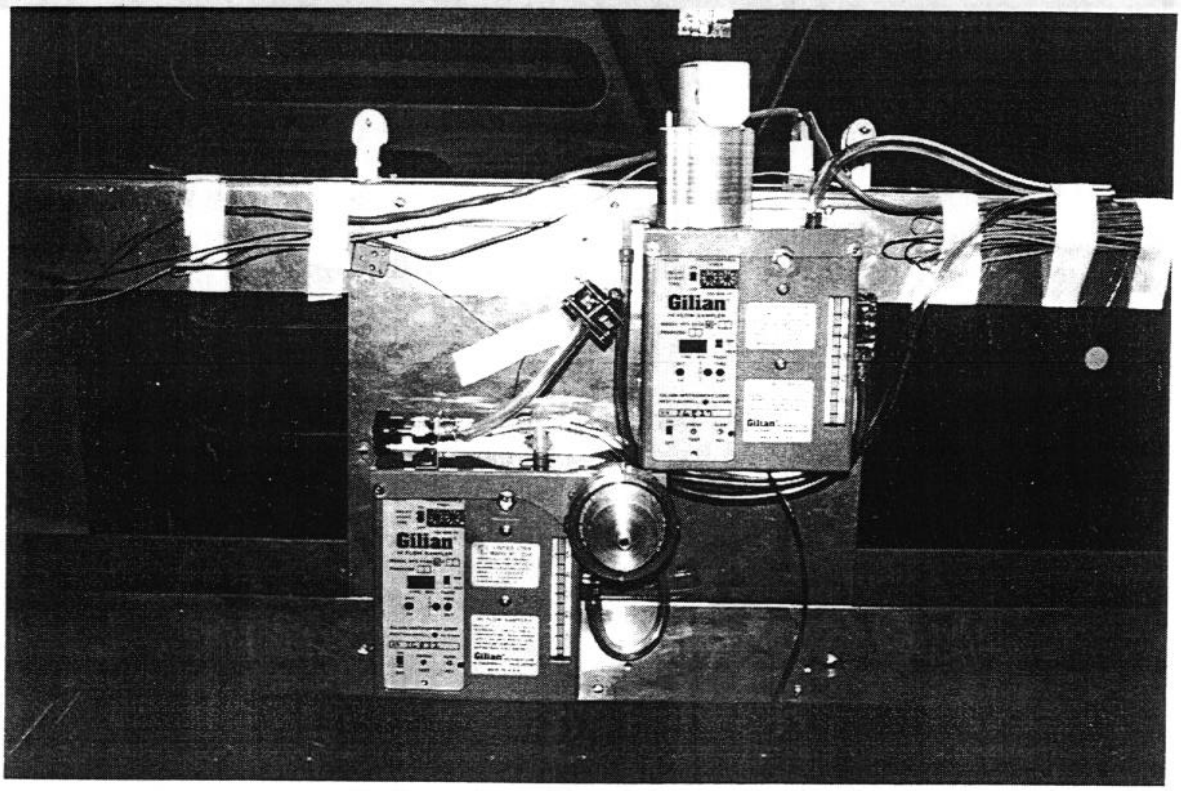

Figure 4. Smoke sampling station used in 1.2 m diameter crude oil laboratory burn

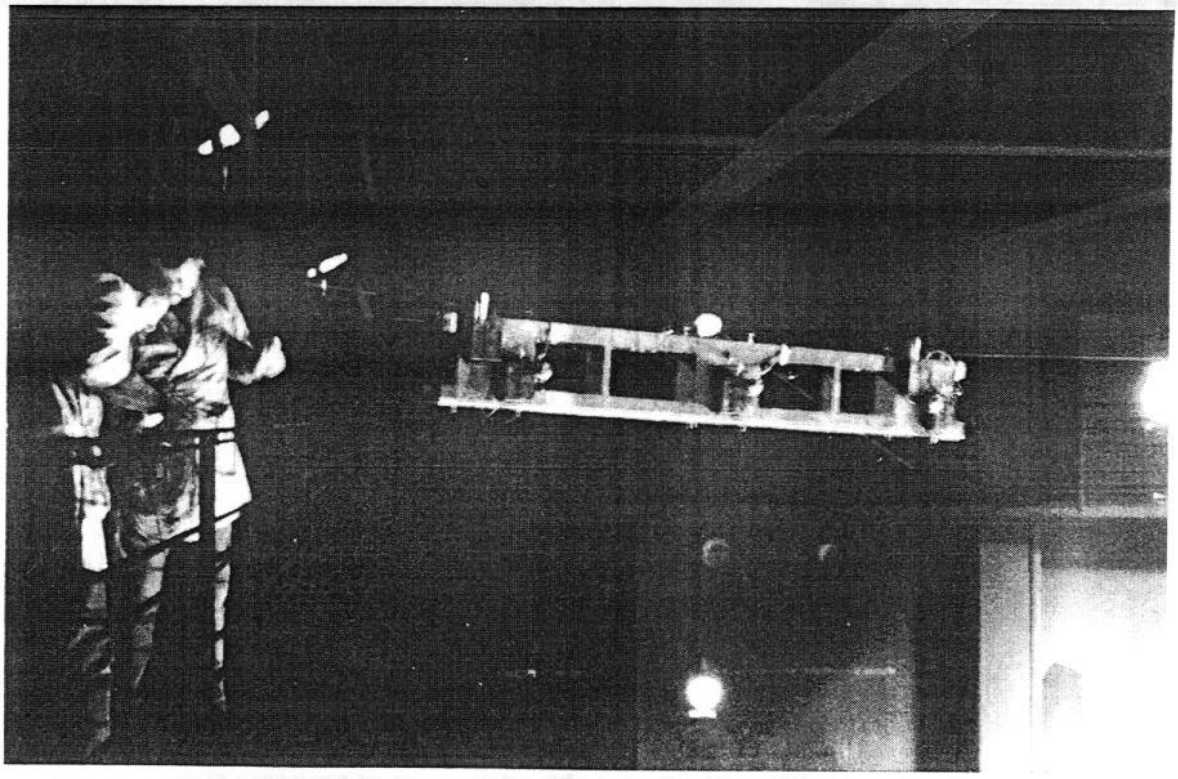

Figure 5. Installation of smoke sampling array in FRI burn hall

The crude oil was stored on a barge which was brought to the site prior to each burn. Oil was pumped through a flexible hose from the barge through the underground piping system and into the pan. The approximate quantity of oil delivered to the pan was monitored with an in-line flow meter. When the quantity of oil delivered to the pan approached the desired quantity, compressed air was pumped from the barge to purge the flexible hose. The barge was then disconnected from the flexible hose and the barge departed the site. The distance from the surface of the oil to the fixed reference point at the top of the pan was recorded and an oil sample was taken. The fixed position and ground based instrumentation and data recording were started and the oil was easily ignited with an extended propane torch. Video cameras were used to record the burn.

When the fire was out, the temperature profile of the water in the inner pan was measured at two locations on opposite sides of the pan. The distance from the surface of the water/oil residue to the fixed reference point at the top of the pan was recorded on the four sides of the pan. The residue was collected with absorbent material and placed in drums for disposal. The quantity of residue was estimated from the volume of the drums filled taking into account the absorbent material and water collected. After four of the burns (1105, 1107, 1109, and 1110), there was a greater quantity of residue than could be readily collected in two or three drums. It is estimated that there was two to three times the quantity of residue then found in the earlier burns due to variations in the extinction process. In these cases to aid in the clean-up, a small quantity of diesel fuel was poured on the residue after it had cooled and the diesel and burn residue mixture was ignited. This procedure was repeated two times for burns 1109 and 1110 until the residue had been reduced to a quantity which could be placed in two drums. The residue was then collected and measured.

LABORATORY BURN PROCEDURE

Prior to pumping crude oil into the pan, fresh water was added to the pan so that the water level was 80 mm below the top of the pan. The output from the pressure transducer was recorded and crude oil was pumped with a hand pump into the pan until an oil thickness of 50 mm was obtained. The crude oil used in the laboratory experiment was the same type Louisiana crude oil used in the mesoscale burns. When 50 mm of oil had been added to the pan the output of the pressure transducer was noted and a calibration for oil depth determined. The manometer data recording was started and the oil was easily ignited with a small flame. Video cameras were used to record the burn.

When steady full pan burning was observed the sampling pumps were started and stopped after 600 seconds and before boiling of the water under the oil started.

Table 3. Mesoscale ground meteorological conditions

Burn No.	Temp. (°C)		Wind Speed (m/s)		Wind Direction (degrees)		Relative Humidity (%)		Barometric Pressure (kPa)		Solar Radiation (kW/m²)
1103 avg.	25.5	24.8	4.1	4.5	171	165	76	76	101.0	101.6	0.70
Minimum	25.2	24.7	2.9	3.2	39	138	73	76	101.0	101.5	0.69
Maximum	25.7	25.1	5.1	6.1	188	187	78	77	101.0	101.6	0.71
1105 avg.	10.7	10.2	4.7	5.0	340	341	69	76	101.4	101.7	0.35
Minimum	10.5	10.0	2.9	3.1	11	27	66	74	101.4	101.7	0.17
Maximum	11.1	10.7	7.0	8.7	269	299	73	78	101.4	101.8	0.79
1106 avg.	11.8	11.3	3.8	3.8	340	339	48	50	102.0	102.3	0.59
Minimum	11.2	10.5	1.8	0.8	20	33	44	48	101.9	102.3	0.14
Maximum	12.5	11.6	6.4	7.0	284	245	53	53	102.0	102.5	0.65
1107 avg.	12.9	12.4	3.6	4.1	3	358	43	46	102.3	102.7	0.62
Minimum	12.6	11.9	2.0	2.5	36	38	41	45	102.2	102.7	0.44
Maximum	13.2	13.0	5.2	7.1	314	322	45	47	102.3	102.8	0.76
1109 avg.	20.3	20.4	2.1	2.2	16	12	55	57	102.1	102.6	0.24
Minimum	19.9	19.9	0.9	0.7	52	41	52	56	102.1	102.6	0.06
Maximum	20.5	20.7	2.8	3.4	342	338	59	57	102.2	102.6	0.56
1110 avg.	19.3	19.2	1.9	2.9	100	100	69	71	102.2	102.6	0.19
Minimum	19.1	18.3	0.4	1.3	19	55	68	69	102.2	102.5	0.15
Maximum	19.6	19.7	3.3	4.6	197	130	71	73	102.2	102.6	0.21

EXPERIMENTAL CONDITIONS

Table 3 gives a summary of the ground and table 4 the airborne meteorological conditions measured during each of the mesoscale burns. The values in the table are averages over the time from ignition to extinction. Wind directions are the direction from which the wind originates with 0° being north. Also shown in these tables are the maximum and minimum values measured during the burn. In table 3 the results for the two ground weather stations are given for each burn. There is generally good agreement between the two stations although there is a consistent difference in the atmospheric pressure. Since the pressure transducer in the weather station in the first column was most recently calibrated it is assumed to be accurate. Although the meteorological conditions varied during the burns, the burns were of relatively short duration and the averages are representative of the actual conditions. The airborne weather data was collected at an elevation of approximately 30 m and previous measurements showed the meteorological conditions to be generally uniform above 20 m [13].

The temperature inside the FRI facility at the start of the burn was 10.4 ±0.3°C. Since the burn was conducted indoors wind measurements were not taken.

Table 4. Mesoscale airborne meteorological conditions

Burn No.	Temp. (°C)	Wind Speed (m/s)	Wind Direction (degrees)
1103 avg.	25.9	7.8	179
Minimum	25.7	6.4	167
Maximum	26.1	8.7	190
1105 avg.	9.0	9.6	352
Minimum	8.7	6.2	39
Maximum	9.4	12.6	260
1107 avg.	10.8	5.7	337
Minimum	10.2	3.2	0
Maximum	11.6	8.6	313
1109 avg.	18.3	3.2	53
Minimum	17.9	1.1	16
Maximum	18.6	4.3	97
1110 avg.	17.7	4.9	82
Minimum	17.6	3.6	63
Maximum	17.9	6.5	101

1106 - Not available

BURNING RATE

The burning of the crude oil was observed to take place in four distinct phases. The four phases were; 1) spreading, 2) steady burning, 3) steady burning with boiling of the water below the oil layer, and 4) transition to extinction. The spreading phase lasted from 80 to 180 s as flames spread over the surface from the single ignition point on the upwind side of the pan to cover the entire fuel surface. Once the entire oil surface was covered with flames, the burning continued at a steady rate until the water below the oil surface began to boil. The onset of boiling was characterized by a noticeable increase in fire generated sound which resembles sizzling and bubbles breaking through the oil surface. During boiling the burning rate increased to a steady rate which was greater than the rate prior to boiling. When the fuel was nearly consumed, the fire began a transition to extinction. This was characterized by areas of the oil surface with no visible flames. Frequently, there were oscillations in the burning behavior with increased and decreased burning area and transition to and from boiling. The burning area decreased toward the downwind side of the pan until

extinction. A brief chronology of the observed burning behavior for each of the burns is given in table 5.

Table 5. Mesoscale burn chronology

Burn No.	Effective Burn Dia. (m)	Initial Oil Depth (mm)	Time to Full Involvement (s)	Time to Begin Boiling (s)	Time to Begin Extinction (s)	Time to Extinction (s)
1103	6.88	61	92	720	1104	1334
1105	17.2	57	180	825	1080	1158
1106	17.2	56	90	730	938	3620
1107	17.2	54	102	627	857	1177
1109	17.2	54	80	600	965	990
1110	17.2	55	91	666	911	1530

Note: All times from ignition

The initial volume of oil was estimated using the liquid surface measurements taken before the oil was added and after the oil was added. Table 6 gives the initial volume of oil, the volume of residue collected, the volume of oil consumed by burning and the percentage of the initial volume of oil consumed by burning. In the cases where the residue was burned before cleanup the number and duration of the residue burns is shown. The oil consumed is the total oil consumed during both the primary and residue burns.

Table 6. Mesoscale oil volume

Burn No.	Crude		Residue		Consumed		Consumed (%)	Residue burns
	(m^3)	(gal)	(m^3)	(gal)	(m^3)	(gal)		
1103	2.26	596	0.02	5	2.24	591	99	none
1105	13.1	3460	0.09	25	13.0	3435	99	1st - 3000 s
1106	12.9	3415	0.11	30	12.8	3385	99	none
1107	12.6	3320	0.09	25	12.6	3295	99	1st - 1440 s
1109	12.5	3290	0.28	75	12.5	3215	98	1st - 1320 s 2nd - 1140 s
1110	12.7	3350	0.28	75	12.7	3275	98	1st - 1140 s 2nd - 360 s

Note: Residue quantities after residue burns if applicable

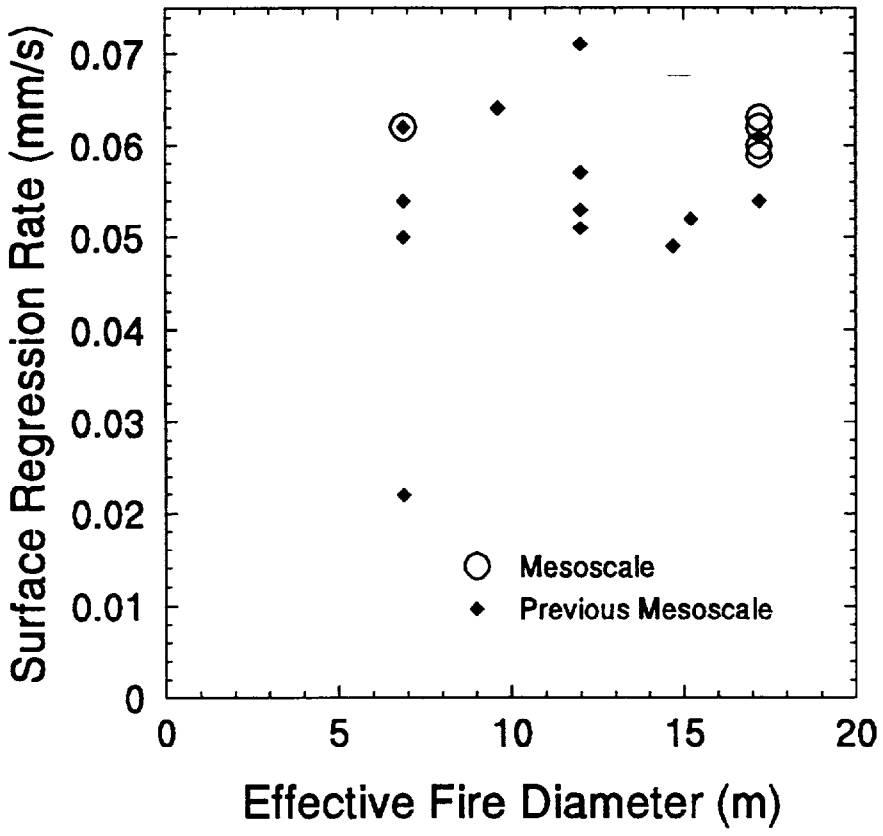

Figure 6. Crude oil surface regression rate for mesoscale burns

The burning rate or the rate at which the oil was consumed during burning was estimated from the liquid level in the pan as measured by the pressure transducer. The output of the pressure transducer was calibrated in salt water and converted to oil depth using the specific gravity of the oil. The specific gravity of the oil was 0.846 ±0.001 as measured using the mechanical oscillator technique with an accuracy of ±0.001. The salt content of the water in the pan was measured before each test using the sodium ion electrode method with an accuracy of ±0.01 %. The salt concentration in percent NaCl and specific gravity of the water in the pan for each burn is given in table 7. The oil surface regression rate was calculated using a least squares linear fit of the pressure transducer output over the time from full pan involvement to the beginning of extinction. The data showed no difference in the burning rate before and during boiling.

The specific mass burning rate (rate of mass loss per unit area) was calculated from the surface regression rate and the density of the oil. The heat release rate was

determined by multiplying the mass loss rate by the effective heat of combustion for the crude oil (41.9 MJ/kg) [13].

Table 7. Water Properties

Burn Number	Salt Concentration (% NaCl)	Specific Gravity
1103	0.84	1.007
1105	0.75	1.006
1106	0.76	1.006
1107	0.74	1.006
1109	0.71	1.005
1110	0.67	1.005

Table 8 shows the mesoscale burning and surface regression rates and the observed burn times. Table 9 gives the same information in engineering units. Figure 6 is a graph of the surface regression rate as a function of the effective burn diameter. From this graph it appears that for the range of diameters used in the mesoscale burns there is no dependency of surface regression rate on burn area. The mean value is 0.062 ± 0.003 mm/s. The mean value for the burning rate per unit area is 0.052 ± 0.002 kg/s/m^2 (5.4 ± 0.2 gal/hr/ft^2) and for the heat release rate per unit area is 2180 ± 100 kW/m^2. The scatter in the regression, burning and heat release rates was due in part to the variable nature of the burns. The wind direction and speed contributed to the wide variation in extinction behavior observed although it did not appear to affect the average burning rate. In mesoscale burns 1103 and 1106 the wind corralled the remaining fuel in a corner of the pan as the fire approached extinction allowing almost all the fuel to be consumed in a small area fire that burned in the corner. These burns are thought to be most representative of results expected from oil burning in a towed boom. Like the wind corralling fuel into the corner of the mesoscale pan, the motion of the towed boom over the water and wind forces would corral oil in the apex of the boom allowing all the oil to be consumed before fire extinction.

Table 8. Mesoscale burning rate

Burn No.	Effective Burn Dia. (m)	Burn Time (s)	Burning Rate ($kg/s/m^2$)	Burning Rate (kW/m^2)	MW	Surface Regression Rate (mm/s)
1103	6.88	1012	0.053	2210	82	0.062
1105	17.2	900	0.054	2240	520	0.063
1106	17.2	848	0.053	2235	515	0.063
1107	17.2	755	0.051	2120	490	0.060
1109	17.2	885	0.052	2180	505	0.061
1110	17.2	820	0.050	2095	485	0.059

Table 9. Mesoscale burning rate (engineering units)

Burn No.	Effective Burn Dia. (ft)	Burn Time (s)	Initial Oil Thickness (in)	Burning Rate ($gal/hr/ft^2$)	Surface Regression Rate (in/min)
1103	22.6	1012	2.4	5.50	0.15
1105	56.4	900	2.2	5.60	0.15
1106	56.4	848	2.2	5.55	0.15
1107	56.4	755	2.2	5.30	0.15
1109	56.4	885	2.1	5.45	0.15
1110	56.4	820	2.2	5.20	0.14

In previous experiments [13] the oil surface regression rate was determined from the liquid level measurements by dividing the quantity of fuel consumed by the burn time from full pan involvement to the beginning of extinction. Table 10 gives the oil surface regression rate determined from the pressure transducer and the measurements of the oil surface level. The average regression rate determined from the liquid surface measurements of 0.064 mm/s is within 5% of the average rate determined from the pressure transducer. The regression rates calculated from the pressure transducer measurements show less variation than the rate calculated from the liquid surface measurements. This comparison indicates that the regression rates calculated from the pressure transducer measurements are more representative of the actual regression rates.

Table 10. Mesoscale oil surface regression rate

Burn No.	Effective Burn Dia. (m)	Surface Regression Rate from Pressure Transducer Measurements (mm/s)	Surface Regression Rate from Liquid Level Measurements (mm/s)
1103	6.88	0.062	0.060
1105	17.2	0.063	0.062
1106	17.2	0.063	0.065
1107	17.2	0.060	0.071
1109	17.2	0.061	0.059
1110	17.2	0.059	0.065

The 1.2 m diameter laboratory fire, after an initial ignition transient, achieved nearly steady burning conditions. Table 11 gives a chronology of the burn. The burning rate or the rate at which the oil was consumed during burning was estimated from the liquid level in the pan as measured by the pressure transducer. The output of the pressure transducer was calibrated with oil depth, and the oil surface regression rate was calculated using a least squares linear fit of the pressure transducer output over the time from full pan involvement to the beginning of extinction. The data showed little difference in the burning rate before and during boiling of the water beneath the oil.

Table 11. Laboratory burn chronology

Burn Dia. (m)	Initial Oil Depth (mm)	Time to Full Involvement (s)	Time to Begin Boiling (s)	Time to Begin Extinction (s)	Time to Extinction (s)
1.2	50	40	970	1000	1368

Note: All times from ignition

From the burning rate, the heat release rate of the fire was calculated by multiplying the mass loss rate of the fuel by the effective heat of combustion of the fuel as described above. Table 12 gives the burning rate for the 1.2 m diameter laboratory burn.

Table 12. Laboratory burning rate

Burn Dia. (m)	Burn Time (s)	Burning Rate (kg/s/m²)	Burning Rate (kW/m²)	MW	Surface Regression Rate (mm/s)
1.2	960	0.039	1630	1.8	0.046

For the 1.2 m diameter burn the burning rate was 0.039 kg/s/m^2, the surface regression rate was 0.046 mm/s, and the heat release rate was 1630 kW/m^2.

SMOKE YIELD MEASUREMENTS

The smoke production from a fire may be expressed in terms of a smoke yield Y_S which is defined as the mass of smoke particulate m_P produced from burning a fuel mass m_F, as:

$$Y_S = \frac{m_P}{m_F} \tag{1}$$

The mass of carbon in the fuel that is consumed by burning is equal to the mass of carbon in the smoke plume.

$$m_{C,Smoke} = m_{C,Fuel} \tag{2}$$

Three assumptions are made in the analysis. The first is that the smoke particulate is predominately carbon. Previous laboratory measurements [10] have shown that the organic carbon fraction of smoke from crude oil pool fires is not greater than 10 percent before there is any boiling in of supporting water sublayer. The remainder of the smoke contains greater than 90 percent elemental carbon. Thus the total carbon content which includes the elemental carbon and the carbon contained in the organic fraction is well over 90 percent of the content of the smoke. Based on this evidence, for the purpose of the smoke yield analysis the smoke particulate is considered to be pure carbon. The second assumption is that samples are collected over a suitable time period to average out natural fluctuations in the fire and plume. In the mesoscale tests and laboratory tests, samples are drawn over a period of 600 to over 1000 seconds. This is deemed sufficient to represent the average burning conditions for the fires. The third assumption is that no preferential separation of smoke particulate and combustion gases occur in the smoke plume up to the point where the sample is taken. In all field measurements, and unconfined laboratory burns, the smoke yield measurement is made close to the source where the smoke and gaseous combustion products move in a well formed smoke plume. Combining equations (1) and (2) and taking into account the three assumptions above yields:

$$Y_S = \frac{m_P}{m_{C,Smoke}} \quad \frac{m_{C,Fuel}}{m_F} \tag{3}$$

To evaluate the above ratio, a known volume of smoke is drawn though a filter and the gaseous portion collected in a sample bag. The mass of carbon in the smoke is equal to the mass of carbon in the smoke particulate plus the mass of carbon in the CO_2 and CO in the smoke. In both the laboratory burn and the mesoscale burns, the concentration of CO in the gas samples were negligible. The smoke particulate mass is determined by weighing the filter. The mass of the carbon in the gas is the grams of carbon per mole of CO_2 (and CO) times the moles of gas sample times the difference in the volume fraction of CO_2 (and CO) in the sample and the background. The volume fraction of CO_2 in the sample and the background were determined using a gas chromatograph. The mass of carbon in the smoke is:

$$m_{C,Smoke} = m_P + 12\frac{g}{mole} n(\chi^S_{co_2} - \chi^B_{co_2}) + 12\frac{g}{mole} n(\chi^S_{co} - \chi^B_{co}) \tag{4}$$

The moles of gas in the smoke sample were calculated using the ideal gas law.

$$n = \frac{PV}{RT} \tag{5}$$

where:
n = moles of gas (mol)
P = atmospheric pressure (kPa)
V = total volume of gas sampled (L)
R = gas constant 8.314 (kPa L/K g mol)
T = ambient temperature (K)

As tested in the laboratory, the flow controllers on the pumps used provide nearly constant mass flow over the range of temperatures experienced in the fire plume so the pressure and temperature in the equation above were taken at the location where the pump flows were calibrated.

The ratio $m_{C,Fuel}/m_F$ is evaluated by determining the elemental carbon mass fraction in the fuel. From the elemental analysis of the Louisiana crude oil, this value is 0.8579.

Combining equations (3) and (4) yields the expression for smoke yield in terms of the measured quantities.

$$Y_S = \frac{m_P \ (m_{C,Fuel}/m_F)}{m_P + 12\ n\ (\Delta\chi_{CO_2} + \Delta\chi_{CO})} \qquad (6)$$

where: $\Delta\chi_{CO_2}$ = difference between the volume fraction of CO_2 in the sample and the background

$\Delta\chi_{CO}$ = difference between the volume fraction of CO in the sample and the background

In the field, smoke was drawn by a battery operated pump through a pre-weighed filter which collected the particulates. The gas passed through the pump to a micrometer adjusted flow control valve and exhaust orifice which metered a portion of the gas flow to a 5 liter sample collection bag. The flow through the filter was measured with a bubble flowmeter prior to each use. The filter samples were weighed on a precision balance before and after the burn and the concentration of CO_2 in the sample collection bag was determined using a gas chromatograph. In the mesoscale burns, the sampling package was suspended below a tethered miniblimp which was manually maneuvered from the ground and held in the smoke plume downwind of the fire. The altitude and range from the fire are given in table 2. A radio controlled switch was used to start and stop the pump remotely as the sampling package was carried into and removed from the fire plume [11]. The sample collection times were nominally 1000 seconds. For the laboratory burn, the sample packages were connected to a cable which extended horizontally 15 m above the fuel. The pumps were started by a switch located at floor level 92 seconds after ignition and run for 600 seconds.

Smoke yields from the mesoscale burns are given in table 13 and from the laboratory burn in table 14. The smoke yields from all burns are shown in figure 7 along with measurements from previous burns[13]. From figure 7 it can be seen that smoke yield is dependent on fire diameter. The yield is generally lower for smaller diameter fires. In small diameter fires the air which is entrained around the fire perimeter more readily mixes with the fuel resulting in more complete combustion and a lower smoke yield. The average smoke yield for the 1.2 m diameter fire (10.9%) as measured in the laboratory is nearly the same as the average yield for the 17.2 m effective diameter mesoscale fires (10.5%).

The controlled laboratory experiment provided the opportunity to evaluate if the smoke yield measurements as performed in the mesoscale tests would yield different values from different radial positions in the smoke plume. Following the assumption that both the gases and the particulate travel together near the fire mixing with the entrained air as the smoke moves away from the source, the smoke yield should be equal when measured at the center of the plume and at its edge. In mesoscale tests, due to variations in the wind, natural fluctuations in the fire, and difficulties in positioning the packages suspended below the blimp, the smoke samples are drawn from a variety of positions within the plume over the long sampling time. Therefore it is important to assure the accuracy of these measurements and that position is not a sensitive factor in the smoke yield measurement.

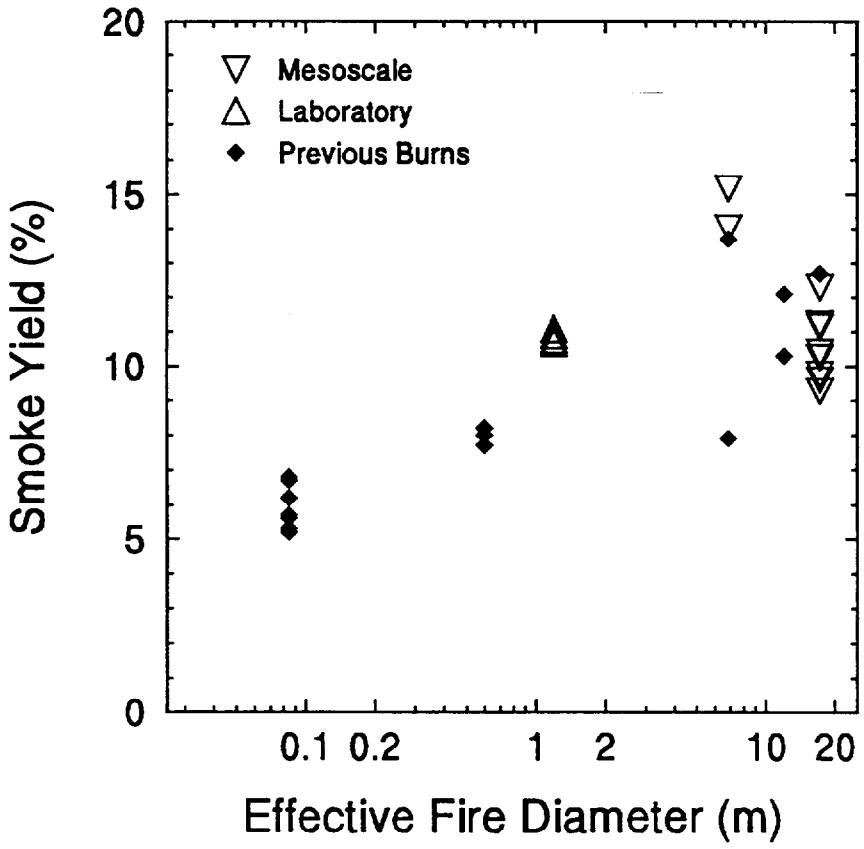

Figure 7. Smoke yield for mesoscale and laboratory burns

In the laboratory burn of a 1.2 m diameter Louisiana crude oil pool fire, the smoke sampling array was positioned manually such that one of the packages was on the centerline of the plume and the other two were positioned radially outward a height of 15 m above the fuel surface. Figure 8 is a photograph of the smoke package in the smoke plume at an instant when the natural puffing of the fire provided a clear view of the entire array of three sampling stations. Observations of the package during the burn showed that the sampling positions on the plume centerline and one meter from it were completely obscured by smoke during most of the burn as seen in figure 3. The third station two meters from the centerline near the visible edge of the plume was only intermittently obscured from sight and drew its sample from predominately lower concentrations of smoke particulate.

Table 14 shows the measured smoke yield from two sample packages at the one and two meter positions and one sample package at the centerline. Only one value is available from the centerline position because the gas sample bag was punctured during processing and the sample was deemed unreliable. The standard deviation of

the smoke yield measurements from the one and two meter positions are 0.16 and 0.22 respectively. Even accepting the smaller of these numbers, all of the measured values for smoke yield are within two standard deviations of the average for all five measurements, 10.9 percent, so that the measurement of smoke yield may be considered independent of radial position in the plume. The relatively small standard deviations for the measurements performed at the same position in the plume show that measurement system for smoke yield has high precision. Smoke yield values are repeatable to within 4 percent of the average value measured in the laboratory environment.

Figure 8. Smoke sampling array (arrow) 15 m above fire during 1.2 m diameter crude oil laboratory burn

Table 13. Smoke yield from mesoscale burns

Burn No.	Effective Burn Dia. (m)	Sample	Start Time[1] (s)	Total Time (s)	Smoke Yield (%)
1103	6.88	1	92	1227	14.0
		2	317	1002	15.2
1105	17.2	1	60	1200	10.3
1106	17.2	1	50	1099	11.1
1107	17.2	1	23	1235	10.4
		2	23	1235	9.9
1109	17.2	1	49	1050	9.4
		2	49	1050	9.6
		3 - boiling	609	490	11.2
1110	17.2	1	41	1508	12.3
		2	41	1508	11.2

1 - Times from ignition

Table 14. Smoke yield from laboratory burn

Location	Smoke Yield (%)
Plume centerline	10.90
1 m radial from plume centerline	10.90
1 m radial from plume centerline	10.68
2 m radial from plume centerline	11.07
2 m radial from plume centerline	10.76

The smoke yield from the partial pan burn 1103 is distinctly higher than the yields from the other burns. This with the data from the previous burns suggests that either the smoke yield is higher for this diameter fire or that there is a characteristic of the 6.88 m diameter fires that has not been accounted for.

PARTICLE SIZE DISTRIBUTION

Particulate size is an important health consideration and also impacts the dynamics of smoke settling. Particulates having an aerodynamic effective diameter less than 10 μm are considered respirable [14] and may be drawn into the lungs with normal breathing. In general small particle sizes have the greatest resistance to settling and can be expected to be carried much further from the burn site than larger particles. In addition to the overall particulate yield from the crude oil fires, it is therefore important to have some knowledge about the particulate aerodynamic size distribution.

There are no means to directly translate the observed irregular shape of smoke particles [11] into aerodynamic effective diameters. The aerodynamic effective diameter of a particle is defined as the diameter of a smooth spherical particle with a unit density of 1000 kg/m^3 (1 g/cm^3) that has the same settling velocity in air. Therefore, the aerodynamic effective diameter of a particle depends on the size, shape and density of the particle. Cascade impactors measure particle size distribution by the amount of particulate deposited on a series of plates. The particulate laden air is drawn through the cascade impactor which consists of a series of stages each having a nozzle and plate. Aerodynamic forces determine the size ranges that will be deposited on the plate in each stage and the sizes that will pass through to other stages downstream. The fraction of the total deposition collected by each stage of the device determines the distribution of the aerodynamic effective diameter of the particles. The small and light weight commercial impactors used in this study contained 8 stages. For cases where a small quantity of particulate is expected, some of the stages may be removed. Each stage of the impactor is characterized by its cutpoint diameter. The cutpoint diameter is the aerodynamic effective diameter that is collected with 50 percent efficiency. Ideally the cutpoint diameter represents the largest diameter particle which will not pass to the next stage but in practice some larger particles do move to the next stage. The cutpoint diameter is a function of the flow rate through the instrument and decreases with increasing flow rate.

For all burns, the impactor was operated at a flow rate of 0.033 L/s with 8 stages and a back-up filter. Table 15 shows the cutpoint diameters for each of the stages in the instrument and the back-up filter [15].

Table 15. Cascade impactor stage cutpoint size diameters

Stage 1 (μm)	Stage 2 (μm)	Stage 3 (μm)	Stage 4 (μm)	Stage 5 (μm)	Stage 6 (μm)	Stage 7 (μm)	Stage 8 (μm)	Back-up Filter
21.3	14.8	9.8	6.0	3.5	1.55	0.93	0.52	0

Figure 9 shows the cumulative size distribution of smoke particulate from the 1.2 m diameter laboratory fire and a 17.2 m effective diameter mesoscale fire(1110). With respect to the measurements from the three radial positions in the 1.2 m diameter burn, no influence of position from the centerline to the edge of the plume at 2 m from the centerline was measured. The size distribution of particulate from the 1.2 m diameter fire also seems to be a good predictor of that found in the mesoscale experiments, as the distributions nearly coincide over the entire measurement range.

Of course, the limited data for only one crude oil does not justify generalization of this result to other situations.

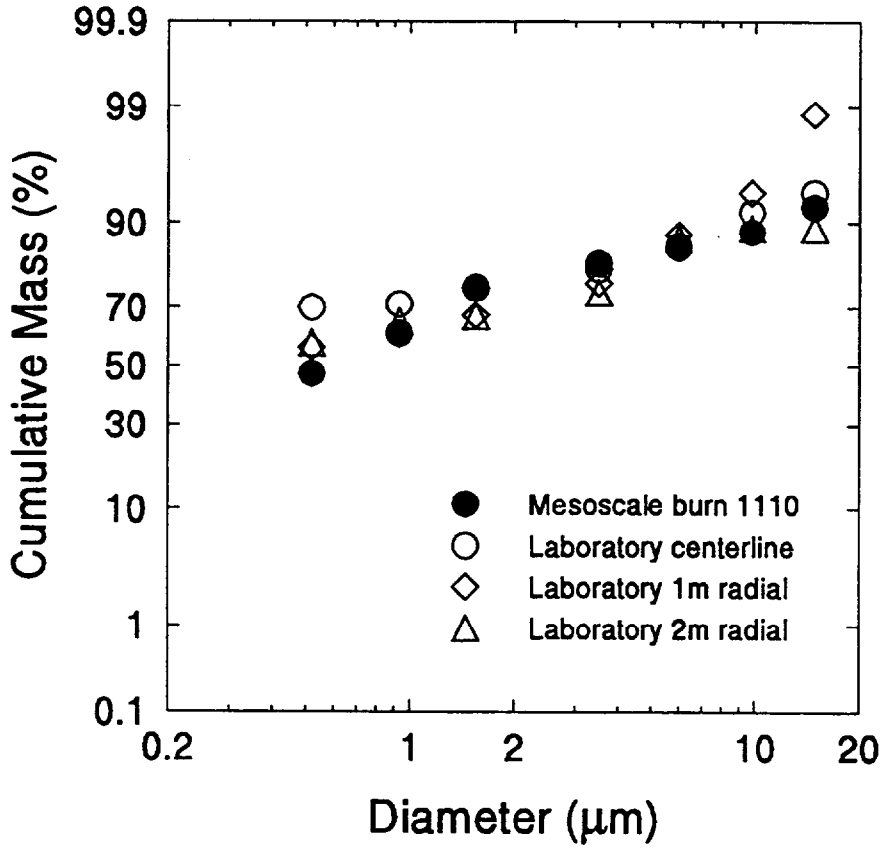

Figure 9. Smoke particulate cumulative size distribution for mesoscale burn 1110 and laboratory burn

WATER TEMPERATURE

Temperatures were measured in the water before and after some of the burns with a portable thermocouple array and in both the oil and water during some of the burns with the fixed thermocouple array in order to quantify the thermal effects of burning oil on the water column. Tables 16, 17 and 18 give the water temperatures measured with the portable thermocouple array. The tables give the time before ignition or after extinction at which the measurements were made and the location of the measurements. All measurements were made approximately 600 mm from the wall of the pan. For the partial pan burn the measurements were made just outside of the boom burn area on the North and West sides of the pan. For the full pan burns the measurements were made at the center of the north and south side of the pan.

Table 16. Water temperature for burns 1103 and 1105

	Burn Number 1103 6.88 m effective diameter				Burn Number 1105 17.2 m effective diameter			
	4066 s before ignition		After extinction time n/a		6690 s before ignition		850 s after extinction	
	North	West	North	West	North	South	North	South
Elevation (mm)	Water temperature (°C)				Water temperature (°C)			
surface (elevation mm)	23.1 (470)	22.9 (485)	24.2 (470)	26.5 (485)	15.9 (485)	15.8 (495)	18.1 (465)	45.0[1] (470)
460	22.8	22.6	24.6	25.6	16.0	16.0	17.5	48.3[1]
380	23.0	22.4	24.7	25.0	16.4	16.0	16.7	20.4
305	22.8	22.3	24.4	24.7	16.1	16.4	16.6	16.9
230	22.9	22.4	24.8	24.8	16.3	16.3	16.3	16.7
150	22.7	22.3	27.9	24.5	16.2	16.1	16.4	16.5
75	22.8	22.3	24.9	24.5	16.2	16.1	16.5	16.5
bottom	22.5	22.4	24.8	24.0	16.1	16.5	16.5	16.5

1 - in oil residue

Table 17. Water temperature for burns 1106 and 1107

	Burn Number 1106 17.2 m effective diameter				Burn Number 1107 17.2 m effective diameter			
	8240 s before ignition		745 s after extinction		5700 s before ignition		1520 s after extinction	
	North	South	North	South	North	South	North	South
Elevation (mm)	Water temperature (°C)				Water temperature (°C)			
surface (elevation mm)	11.9 (465)	11.3 (465)	18.5 (460)	14.3 (450)	12.2 (460)	11.9 (460)	17.8 (460)	55.5[1] (460)
460	12.3	12.2	-	-	-	-	-	-
380	12.2	12.8	14.2	14.2	12.4	12.7	14.8	17.9
305	12.0	12.4	13.9	14.3	12.3	12.7	13.6	12.8
230	12.0	12.7	13.7	14.2	12.4	12.6	13.0	12.9
150	12.4	12.7	13.2	14.3	12.0	12.8	13.0	12.7
75	12.5	12.4	13.3	14.3	12.4	13.0	12.9	12.8
bottom	12.7	12.3	13.7	14.3	13.0	13.0	13.2	13.0

Table 18. Water temperature for burns 1109 and 1110

	Burn Number 1109 17.2 m effective diameter				Burn Number 1110 17.2 m effective diameter			
	7650 s before ignition		1260 s after extinction		6260 s before ignition		1210 s after extinction	
	North	South	North	South	North	South	North	South
Elevation (mm)	Water temperature (°C)				Water temperature (°C)			
surface (elevation mm)	15.6 (470)	16.7 (470)	42.2 (465)	68.4[1] (480)	18.3 (480)	18.4 (480)	53.1 (480)	59.0[1] (480)
460	15.0	15.8	34.5	53.9[1]	18.1	17.7	41.8	44.5
380	15.0	15.8	16.1	16.5	18.1	18.0	18.0	18.2
305	14.8	15.2	15.9	16.5	17.9	17.7	17.8	18.2
230	15.0	15.5	15.4	16.1	18.1	18.0	17.8	18.2
150	15.1	14.7	15.2	16.4	18.1	17.7	17.9	18.0
75	15.3	14.7	15.2	18.5	18.2	18.1	17.8	18.2
bottom	15.4	14.4	15.1	16.4	18.5	17.8	17.7	18.2

1 - in oil residue

The thermocouple array was placed on the bottom of the pan and the elevation of the measurement points is with respect to the bottom of the pan. A temperature measurement was made at the water surface and the approximate elevation of the water surface is indicated in parentheses. The variation in the elevation of the water is primarily due to the uneven bottom of the pan and to a lesser extent the movement of the pan during the burn and wind induced movement of the water. As a result, although the vertical measurement locations reflect the local elevation within ±2 mm, the difference between the elevation measured and the elevation of a level plane is estimated to be within ±12 mm.

The water temperature measurements with the portable thermocouple array show that the water temperature in the pan was uniform with depth and uniform across the pan. The water temperature in the burn area after the fire generally increased 5-40°C within 35 mm of the surface, 1-4°C, 70-115 mm below the surface, and increased 2°C or less at distances greater than 145 mm below the surface. Temperatures in the oil residue were 10-30°C higher than the expected water temperature at the same location. In most cases the water temperatures after the fire reflect the influence of the wind direction on the flames with the temperatures being hotter on the downwind side.

These water temperatures are in agreement with prior measurements and analysis [16] which indicate the thermal penetration rate into the water is slow when compared to

the oil surface regression rate and high temperatures in the water are limited to 35-50 mm below the surface. The thermal penetration of the water is nearly the same for longer burns with thicker oil layers since the temperature in the water does not begin to rise significantly until the burning oil surface nears the water surface.

GROUND LEVEL CARBON DIOXIDE CONCENTRATION

Ground level measurements of CO_2 concentration were made at two locations directly downwind of each of the burns and at one location upwind of burns 1103 and 1105. At regular time intervals air samples at each of the sampling locations were rapidly pumped into a gas sample collection bag and smoke conditions at the sample location noted. The samples included one prior to the start of the burn and one after the completion of the burn to determine the background conditions. After the burn was completed the samples were analyzed at the burn site using a portable gas chromatograph. The chromatograph was calibrated each day using a reference gas with a known CO_2 concentration of 528 ppm.

Tables 19 through 24 show the downwind ground level measurements of CO_2 concentration and the observations at time the gas sample was taken. The times given are from ignition. Although the observation of smoke is subjective, the observer noted whether the smoke was relatively light or dense and if the smoke was continuously present. In many cases the smoke was variable, indicating that the concentration of smoke was rapidly changing as the sample was taken.

Table 19. Ground Level CO_2 Concentration for Burn 1103

24 m Downwind			32 m Downwind		
Time (s)	CO_2 (ppm)	Observations	Time (s)	CO_2 (ppm)	Observations
-1246	338	background	-1126	338	background
14	342	light smoke	74	342	light smoke
314	442	dense smoke	434	395	dense smoke
734	419	dense smoke	854	357	dense smoke
1154	482	dense smoke	1214	402	dense smoke
1274	371	light smoke	1334	337	light smoke

Table 20. Ground Level CO_2 Concentration for Burn 1105

30 m Downwind			45 m Downwind		
Time (s)	CO_2 (ppm)	Observations	Time (s)	CO_2 (ppm)	Observations
-3870	345	background	-3810	344	background
30	381	light smoke	90	366	variable smoke
330	519	dense smoke	390	358	variable smoke
630	348	variable smoke	750	345	variable smoke
930	348	variable smoke	990	349	variable smoke
1050	349	light smoke	1170	362	light smoke
1230	342	clear	1290	343	clear

Table 21. Ground Level CO_2 Concentration for Burn 1106

30 m Downwind			45 m Downwind		
Time (s)	CO_2 (ppm)	Observations	Time (s)	CO_2 (ppm)	Observations
-1155	354	background	-1275	356	background
45	351	clear	105	355	clear
225	362	variable smoke	285	349	clear
405	651	dense smoke	465	367	variable smoke
585	382	variable smoke	645	395	variable smoke
765	379	variable smoke	825	369	light smoke
885	465	variable smoke	1005	357	light smoke
1065	376	light smoke	1125	357	light smoke
1245	385	variable smoke	1305	361	light grass smoke
1425	357	clear	1485	353	light grass smoke
3705	358	clear	3765	349	clear

Table 22. Ground Level CO_2 Concentration for Burn 1107

30 m Downwind			45 m Downwind		
Time (s)	CO_2 (ppm)	Observations	Time (s)	CO_2 (ppm)	Observations
-363	355	background	-303	357	background
-3	353	light smoke	57	350	light smoke
177	382	variable smoke	237	368	variable smoke
297	392	light smoke	417	353	variable light smoke
537	367	variable smoke	597	358	light smoke
657	393	dense smoke	777	360	variable smoke
837	350	variable smoke	897	351	variable light smoke
957	346	variable light smoke	1017	347	clear
1137	349	light smoke	1197	342	clear
1317	351	clear	1377	344	clear

Table 23. Ground Level CO_2 Concentration for Burn 1109

30 m Downwind			45 m Downwind		
Time (s)	CO_2 (ppm)	Observations	Time (s)	CO_2 (ppm)	Observations
-630	349	background	-552	348	background
30	349	light smoke	90	350	clear
167	350	variable light smoke	235	352	clear
300	353	clear	359	377	clear
445	349	clear	518	343	clear
603	355	light grass smoke	670	340	clear
739	351	very light smoke	807	342	clear
885	350	clear	960	344	clear
1023	346	clear	1082	342	clear
1155	343	clear	1258	343	clear

Table 24. Ground Level CO_2 Concentration for Burn 1110

30 m Downwind			45 m Downwind		
Time (s)	CO_2 (ppm)	Observations	Time (s)	CO_2 (ppm)	Observations
-1129	344	background	-1029	347	background
6	344	clear	64	344	clear
131	357	light smoke	198	345	clear
266	348	light grass smoke	334	345	light smoke
418	349	light smoke	491	349	clear
557	352	light smoke	626	346	clear
696	353	light smoke	761	342	light grass smoke
821	349	variable light smoke	881	340	clear
936	348	light smoke	1001	347	clear
1067	353	light smoke	1141	342	clear
1586	344	clear	1656	344	clear

There was sufficient wind speed during the series of burns to cause the smoke plume to tilt towards the ground. The wind speed and direction varied during the burns and the interaction of the wind with obstructions near the pan and the fire plume resulted in unquantified disturbances to the air flowing across and around the pan. As a result, the smoke plume would intermittently plunge towards the ground during the burns exposing instrumentation immediately downwind of the pan to gases and particulate in the smoke plume. Further, ground vortices were occasionally observed originating near the pan and moving downwind along the ground. Figure 10 shows the wind driven smoke plume for burn 1106 as normally it would be expected to be rising from the pan driven in the downwind direction. Figure 11 shows one of the intermittent excursions of the smoke plume to ground level during burn 1106 submerging instrumentation in a portion of the smoke plume. This resulted in smoke frequently being visible at ground level at the two downwind measurement locations. There is excellent correlation between the measured CO_2 concentrations and the observations in that the higher measured concentrations correspond to the observations of denser smoke (figure 11). Further, when clear conditions were observed the measured CO_2 concentrations correspond to the background readings (figure 10). For burns 1103 and 1105 CO_2 concentrations were measured upwind at 45 and 30 m respectively. No smoke was observed at the upwind locations and the CO_2 concentrations remained at the background level. Upwind measurements were not made for the remaining burns so that additional measurements could be made at the downwind locations.

The measurements and observations lead to the conclusion that concentrations of CO_2 above background are only found at ground level when the smoke is observed at ground level. That is to say that elevated levels of CO_2 were only found in the smoke plume.

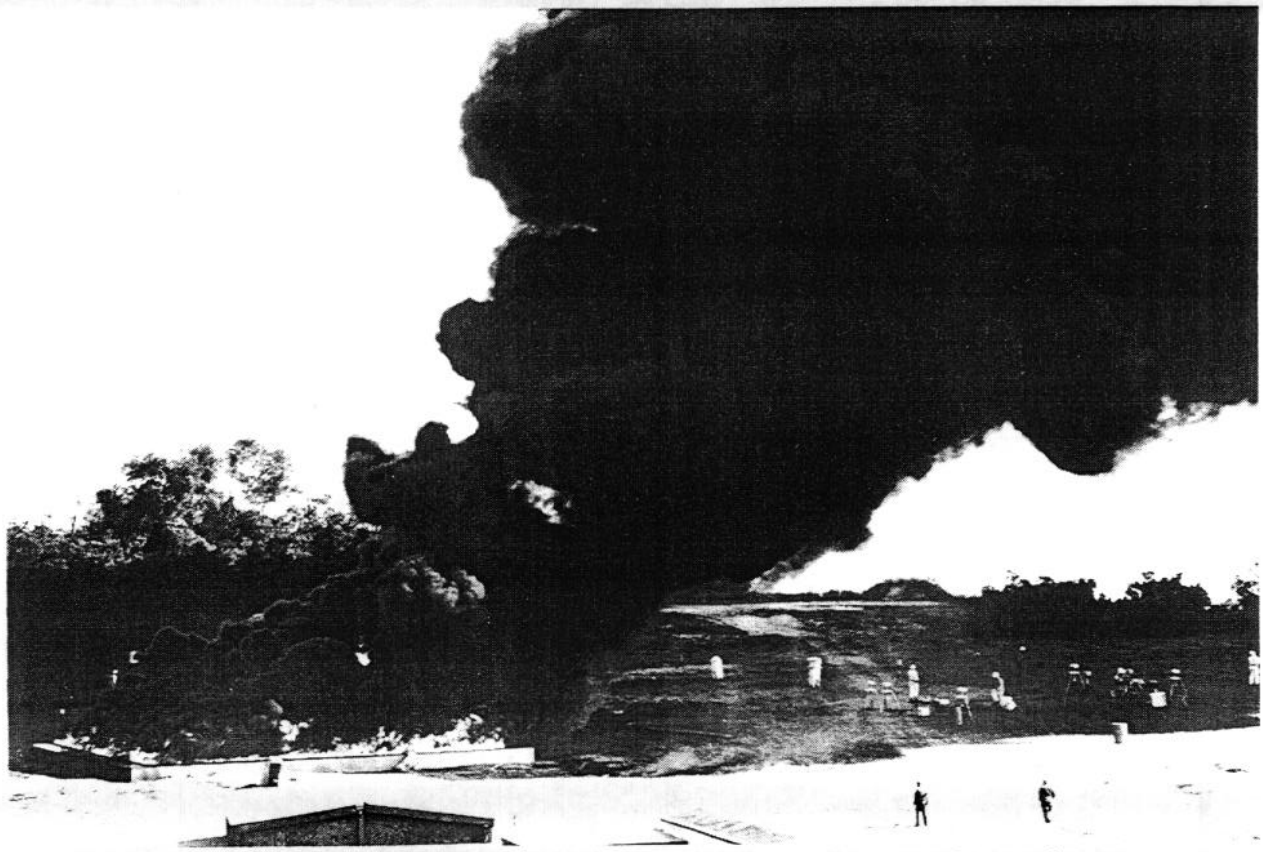

Figure 10. Mesoscale burn 1106 with smoke above the ground near the pan

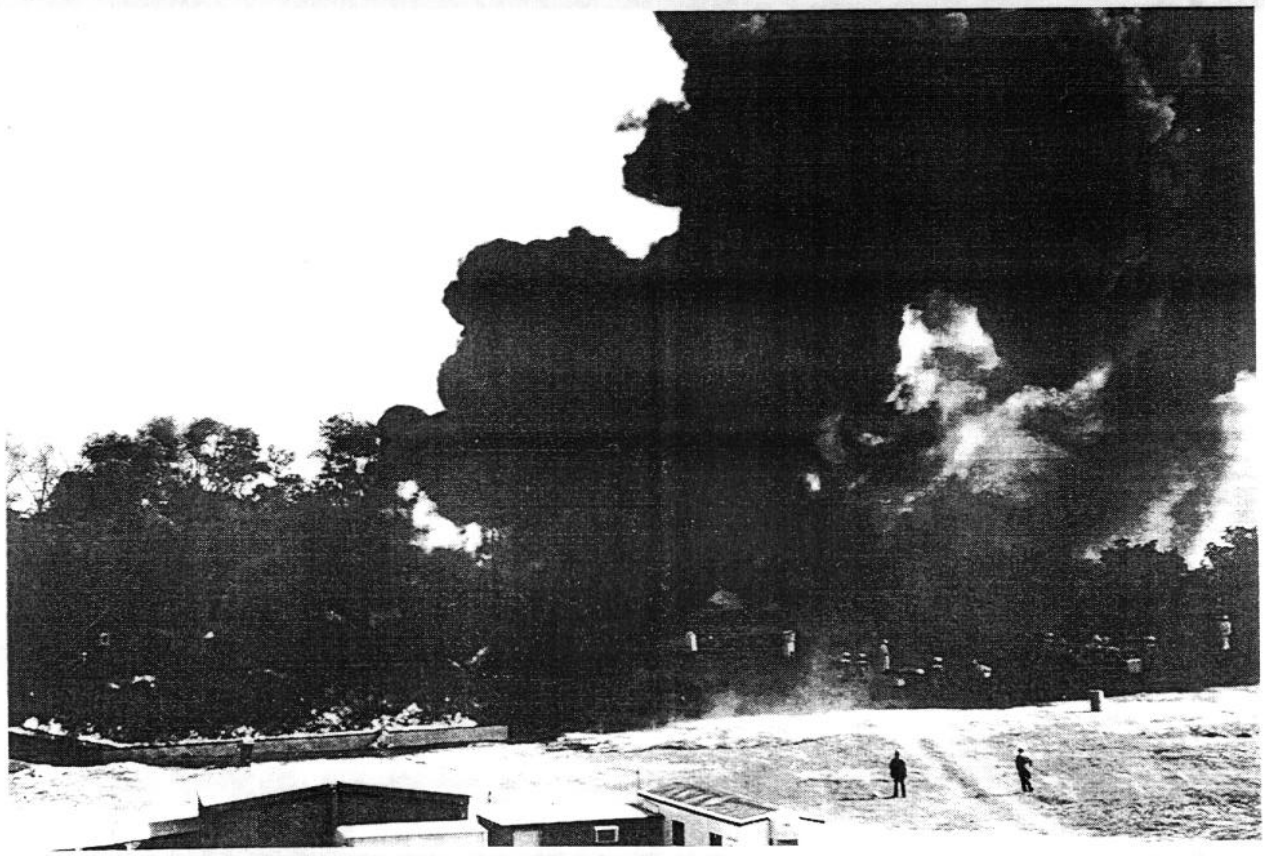

Figure 11. Mesoscale burn 1106 with smoke at ground level near the pan

VISIBILITY OF SMOKE PLUMES

One of the factors influencing the acceptance of in situ burning as an oil spill response method is the visual appearance of the smoke plume from the burning. A highly visible smoke plume, for example, would be expected to elicit a stronger public concern than a barely visible smoke plume regardless of the chemical composition. In part to quantify the appearance of smoke plumes from burning crude oil under various atmospheric conditions and viewing positions and in part to explore means to quantify smoke emissions from observations, the visibility of smoke plumes in the atmosphere was studied. This study utilized previous measurements of visible light attenuation characteristics of smoke [9] and data from mesoscale experiments [13].

The visible characteristics of smoke plumes have long been a segment of air pollution regulations. [17] While the physical appearance of the plume is not directly related to the plume's composition, the United States Environmental Protection Agency (EPA) regulates light attenuation characteristics of smoke at the point of discharge from stationary sources. In general, a smoke plume is considered "clear" to "nearly clear" if the level of visible light obscuration is less than 20 percent, and considered "aesthetically pleasing" if the obscuration level is less than 40 percent [18]. The magnitude of light attenuation due to smoke particulate in the atmosphere may be derived from the following expressions [19, 20]:

$$D = -10 \log_{10}(I/I_0) \tag{7}$$

$$Percent\ Obscuration = [1-(I/I_0)]\times 100 \tag{8}$$

where: D = optical density
I = light intensity after travelling through the smoke
I_0 = initial light intensity

Previous research at NIST involving smoke particulate generation characteristics of crude oils has resulted in expressions for optical density per meter of path length [9]. Given the particulate concentration within the plume, the optical density per meter can be found from the following equation:

$$\frac{D}{L} = 3300 \times \rho_{sp} \tag{9}$$

where: D = optical density
L = optical path length (m)
ρ_{sp} = particulate density (kg/m^3)

The smoke plumes from previous mesoscale experiments have been analyzed using digital image processing techniques [21]. Image processing of the visible plume for

burn 5/30 resulted in its physical dimensions and location in relation to the fire. The same data has been analyzed further to derive the optical path length of light passing through the plume to the observer. The plume dimensions are also used to calculate the average particulate density at various positions in the plume (Figure 12).

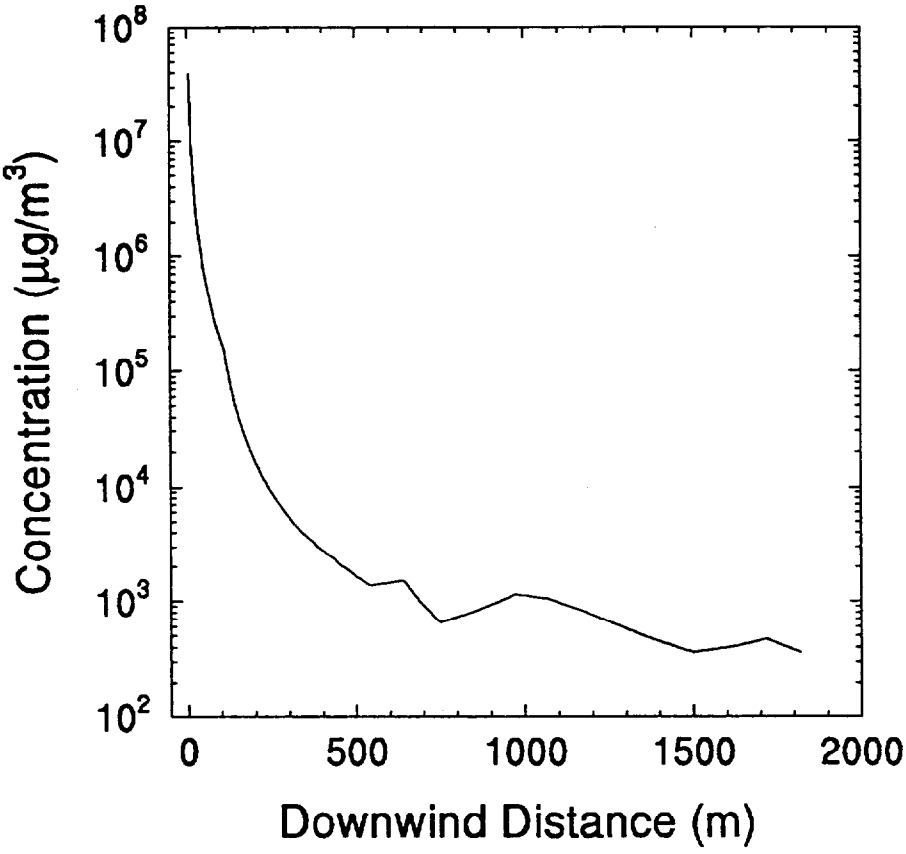

Figure 12. Smoke particulate concentration for mesoscale crude oil burn 5/30

The approximate opacity of the smoke plume may be derived in terms of percent obscuration. In order to predict how the plume may look to a distant observer, however, the opacity of the plume must be converted to a level of contrast between the target plume and its background. This contrast term incorporates the characteristics of the plume, the conditions of the atmosphere, the luminance of the background, and the visual response of the human eye.

The inherent contrast of the plume, which is equal to the light attenuation (opacity) found from equation 8, must be adjusted for reductions in contrast as a result of atmospheric and background effects. The reduction in contrast is caused by daylight scattered into the sight path, and by scattering and absorption of the light from the target. The reduction in contrast is given by the contrast transmittance,

$$T = \frac{C_R}{C_0} \tag{10}$$

where C_R is the apparent contrast realized by the observer at position R, and C_0 is the inherent contrast [22].

In order to find the contrast transmittance term, it is necessary to know the effects of the atmosphere on the plume visualization. Atmospheric haze effects are represented by an atmospheric transmission coefficient, β_0, which is derived from the daylight visual range, D, in meters [22]:

$$\beta_0 = \frac{2.99 \times 10^{-3}}{D} \quad (m^{-1}) \tag{11}$$

The daylight visual range or visibility is a commonly used meteorological term. It is defined as the distance at which a large, dark object is just visible when placed on the horizon. This corresponds to a contrast transmittance of 5 percent.

The effects of various backgrounds are incorporated with the use of a sky-ground or sky-cloud ratio term, B_{hs}/B_b, that corrects for luminance level differences between the horizon sky, B_{hs}, and the background immediately behind the target, B_b. Values of this ratio are provided by previous researchers for several ground and sky conditions [22].

Various expressions for contrast transmittance are given in the literature [22]. These equations take into account the daylight visual range, viewing distance, viewing geometry, and the target background. An example of one such expression, which is applicable for viewing a smoke plume against a cloudy sky, is given by:

$$T = \frac{1 + \frac{B_{hs}}{B_b} \times (\exp \beta_0 [\bar{R}_{R-b} - \bar{R}] - 1)}{1 + \frac{B_{hs}}{B_b} \times (\exp [\beta_0 \bar{R}_{R-b}] - 1)} \tag{12}$$

where: $\bar{R}$ = the distance from the observer to the target
$\bar{R}_{R-b}$ = the distance from the observer to the cloudy background

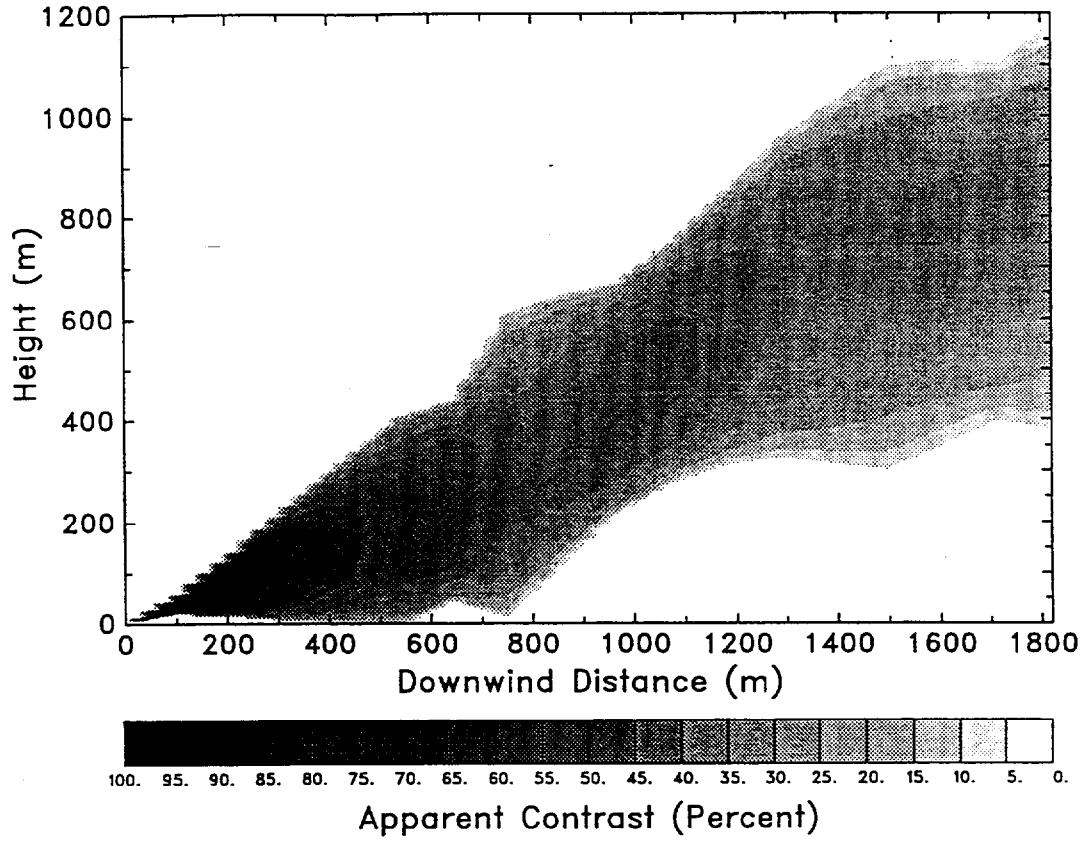

Figure 13. Calculated elevation view of the plume as viewed by an observer located 3.5 km from the fire with the atmosphere devoid of clouds. The atmospheric visibility range is 48 km.

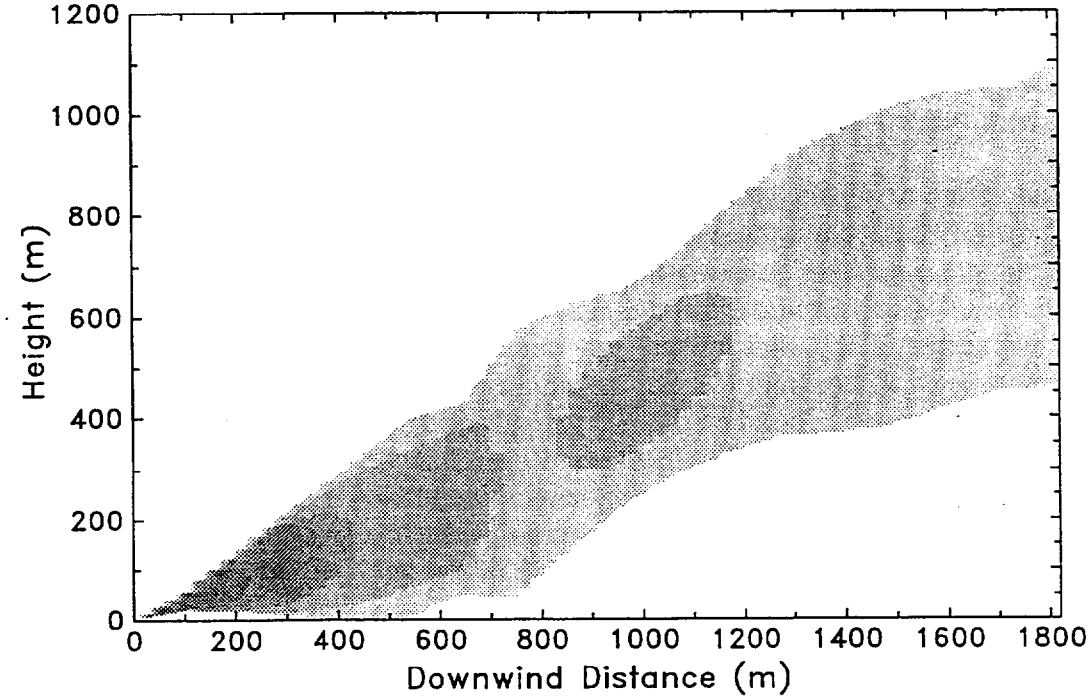

Figure 14. Calculated elevation view of the plume as viewed by an observer located 3.5 km from the fire with the atmosphere uniformly overcast with stratocumulus clouds at an altitude of 2 km. The atmospheric visibility range is 8 km.

The above analysis was employed to find the apparent contrast of a smoke plume under specific conditions. A mesoscale crude oil burn conducted by NIST on May 30, 1991 (burn 5/30) was originally viewed on a clear day, against a blue sky [13]. To this observer located 3.5 km from the fire, the plume would look like the plume in figure 13 where the darker areas correspond to "blacker" smoke. The question may be posed, however, as to what an observer would see on a slightly hazy day with an overcast sky of strato-cumulus clouds at a typical altitude of 2 km [23]. Using equations (7-12) and solving for the apparent contrast C_R, results in a plume which would appear to an observer as is illustrated in figure 14. Notice that much less of the plume is visible, with the plume disappearing somewhere between an apparent contrast of 0 to 20 percent less than 2 km from the source.

In the future, this methodology may be further refined and applied to the output of the LES plume dispersion model. Given the smoke particulate concentration and dimensions of the plume from the model, the visibility of the smoke plume may be predicted. This may be useful in determining the possible appearance of smoke plumes from in situ burning in advance of a proposed burn for the benefit of local authorities making response decisions.

DOWNWIND SMOKE PLUME TRAJECTORY OBSERVATION

The mesoscale burning experiments have provided the opportunity for scientists at NIST and other laboratories to study the near field environment surrounding an in situ burn of crude oil by making measurements in the area surrounding the pan. Since the burn facilities are located on an island, there is limited downwind distance that can be sampled from the island. In all of the mesoscale tests ground based measurements from the island have been limited to 45 m distance downwind. Video images of the smoke plume 3.5 km from the island provided a quantitative measurement of the plume trajectory downwind for approximately 2 km.

In an effort to obtain qualitative information about the appearance of the plume downwind of the burn, during experiment 1105, observers followed the plume from the burn as it traveled downwind using a USCG HH865 "Dolphin" helicopter. At a distance of 10 km from the pan the head of the smoke plume could just be detected by eye against a sky with broken grey clouds. At the time when the head of the plume was at 10 km from the pan the smoke plume extended back towards the pan for 6 km, figure 15. Based on the 900 seconds duration of fully involved burning for that fire and the measured average wind speed of 9.6 m/s during the burn from Table 4, the expected smoke plume length would be 8.5 km. The observed 6 km length is consistent with this estimate considering the possible variations in wind speed with altitude and distance downwind of the test site. As measured from the helicopter, the nominal depth of the smoke plume was 300 m with a varying width of 0.8 km to 1.6 km.

The smoke plume from a similar mesoscale burn, 1107, was photographed extensively as it traveled downwind from the island. These photographs are shown in figures 16 through 19. In figure 16, the black smoke is emitted from the burn and travels

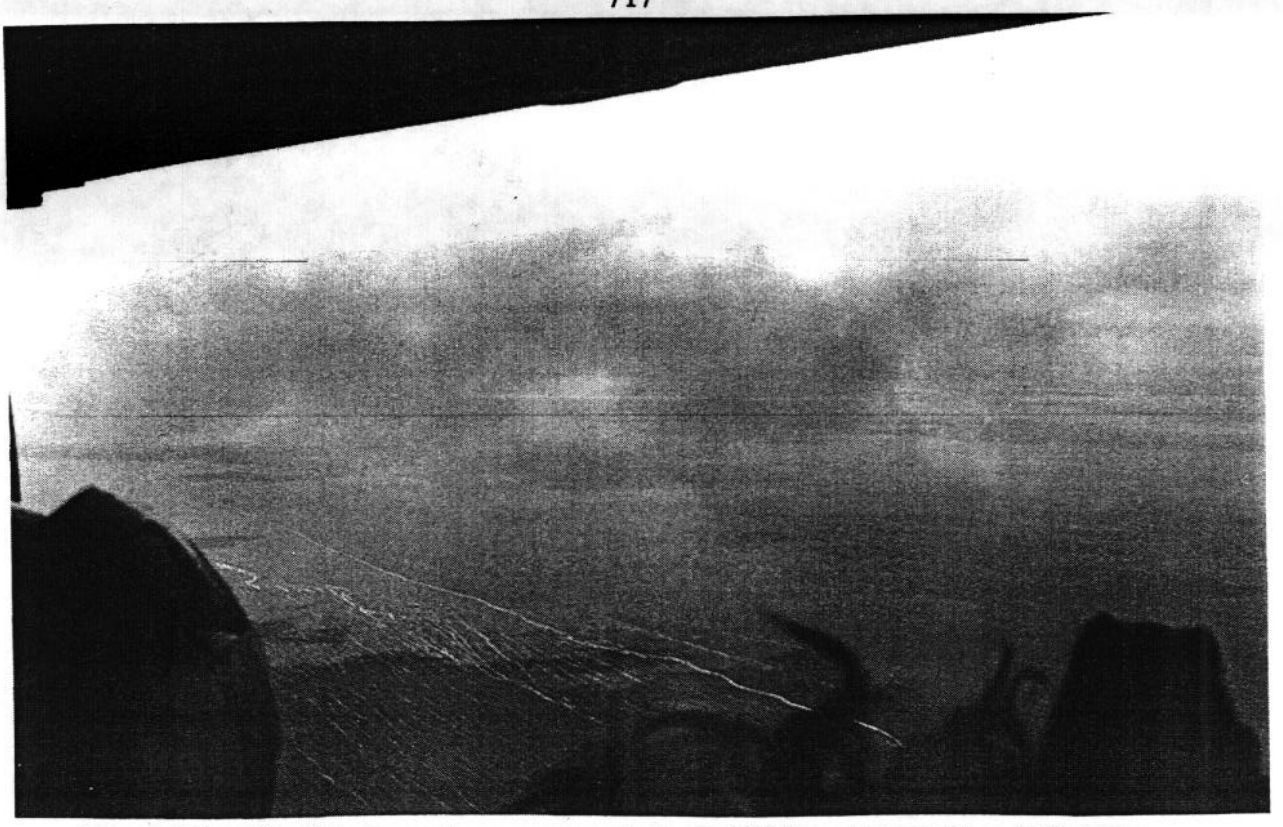

Figure 15. Smoke plume from mesoscale burn 1105 as viewed from helicopter approximately 10 km downwind looking upwind towards the test site

downwind. Figure 17 is 60 s after fire extinction showing the smoke plume as viewed from the rear as it moves downwind. One might also note that some private observers seen in the lower right of the photograph just offshore in a small boat from which they viewed the burn. Figure 18 shows the plume at 500 s after extinction and figure 19 at approximately 1200 s after extinction. At this time the smoke plume, even viewed along its greatest depth from the end on presents only a slight darkening of the background grey sky.

These qualitative observations of the smoke plume do not provide the quantitative data that will be necessary to validate plume trajectory and deposition modeling presented in the next section. The observations do suggest that the smoke plume from mesoscale size crude oil burns may not be a concern based solely on visual observations at distances greater than approximately 10 km from the burn.

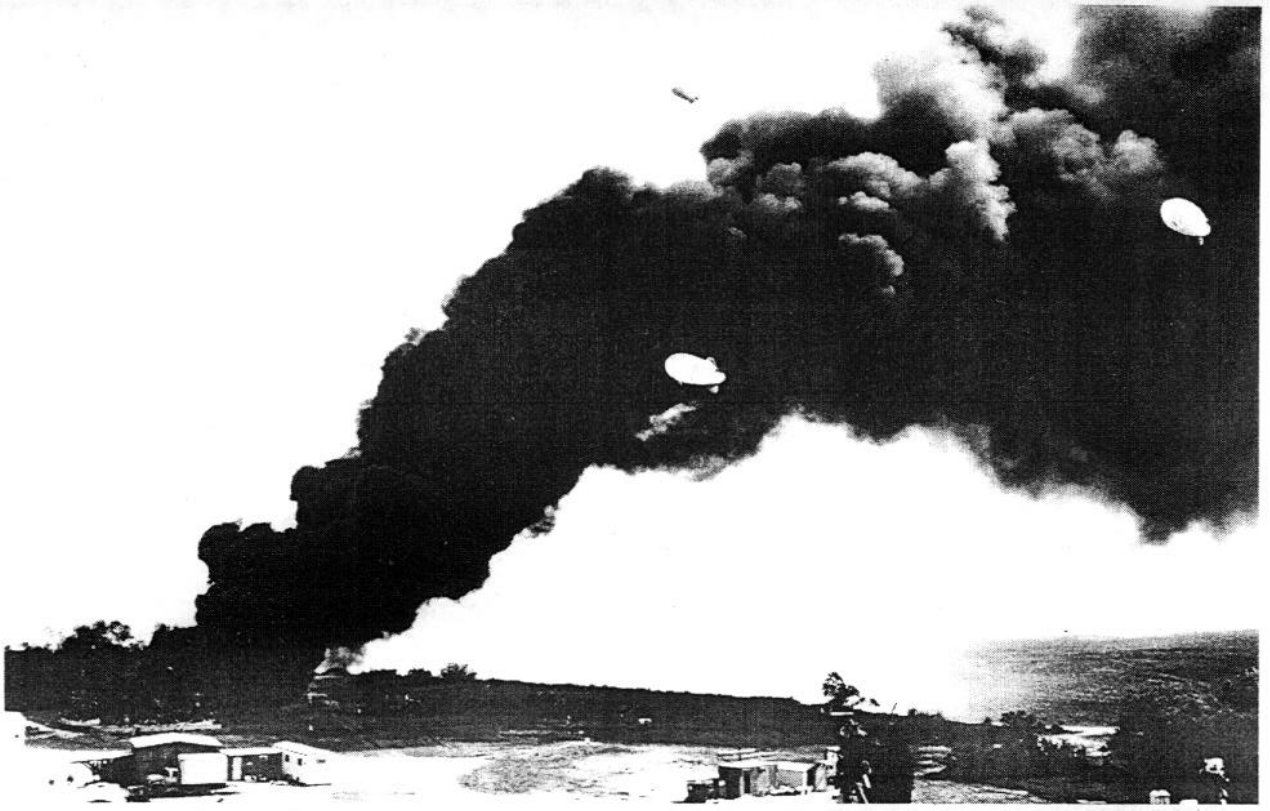

Figure 16. Smoke plume from mesoscale burn 1107 as seen near the pan

Figure 17. Smoke plume from mesoscale burn 1107 moving downwind 60 s after extinction as viewed from the test site

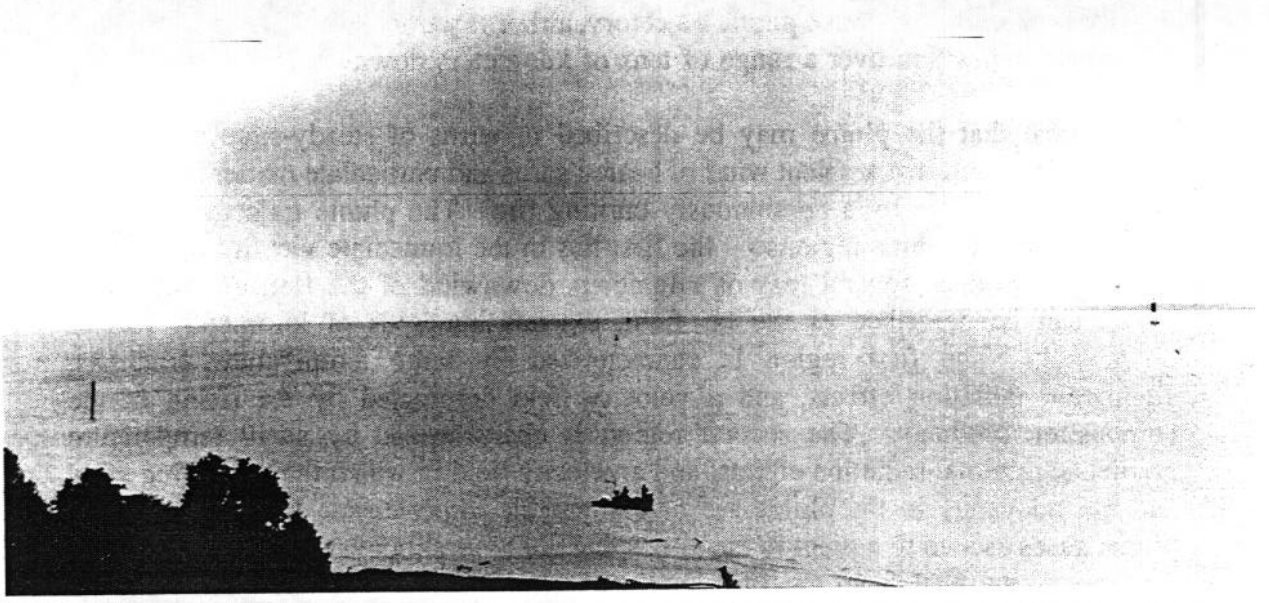

Figure 18. Smoke plume from mesoscale burn 1107 moving downwind 500 s after extinction as viewed from the test site

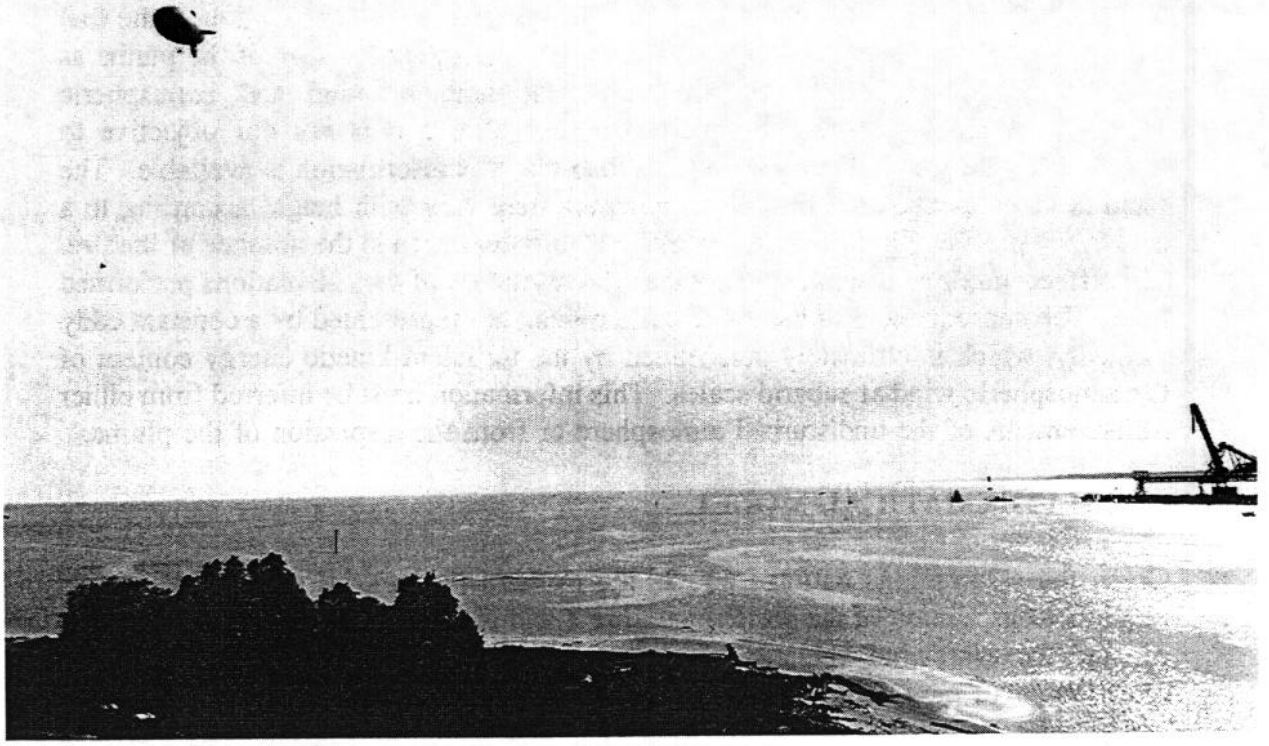

Figure 19. Oval shaped smoke plume from mesoscale burn 1107 appears near the horizon 1200 s after extinction as viewed from the test site

SMOKE PLUME TRAJECTORY MODELING

A principal concern in the decision to use in situ burning as an oil spill response technique is the anticipated trajectory of the plume and the settling out of particulate matter. The Large Eddy Simulation (LES) model is being developed by NIST to provide predictions of smoke plume trajectory, airborne particulate concentrations, and particulate deposition over a range of tens of kilometers downwind of a burn.

We assume that the plume may be described in terms of steady-state convective transport by a uniform ambient wind of heated gases and particulate matter introduced into the atmosphere by a continuously burning fire. The plume trajectory may be broken down into three regions --- the first lies in the immediate vicinity of the fire, the second extends several tens of kilometers downwind of the fire, and the third, which can be described as the far field, extends hundreds of kilometers further downwind. The first region is characterized by large temperature gradients, significant radiation effects, and a velocity field dominated by the rising of the combustion products. The second region is characterized by small temperature gradients, minimal radiation effects, and a velocity field in which the prevailing wind and the buoyancy in the plume are of comparable importance. In this region the plume gases ascend to a point in the atmosphere of neutral buoyancy, and then slowly descend as the heat from the fire dissipates. In the third region, or far field, the descent, dispersion, and deposition of the combustion products is governed by the regional meteorological conditions rather than the fire.

The Large Eddy Simulation of the smoke plume trajectory described below is appropriate for the second region. For this reason it is not necessary to describe the fire in detail, provided that the overall rate of heat release and the fraction of the fuel converted to particulate matter are known. The subsequent location of the plume as it is carried downwind is determined by the ambient wind and atmospheric stratification along the trajectory of the plume. Since it is not our objective to calculate the local meteorology, it is assumed that this information is available. The wind is taken as uniform, but the temperature may vary with height according to a prescribed profile. Finally, the atmosphere is turbulent even in the absence of the fire. This effects mixing on scales smaller than the resolution of the calculations performed here. The consequences of the small scale mixing are represented by a constant eddy viscosity, which is ultimately determined by the turbulent kinetic energy content of the atmospheric wind at subgrid scales. This information must be inferred from either measurements of the undisturbed atmosphere or from the dispersion of the plume.

LES MATHEMATICAL MODEL

Given the assumptions outlined above, the mathematical model of a smoke plume requires a description of the gas temperature T and pressure P, the particulate density ρ_p, and the crosswind velocity components (v,w) in a plane (y,z) normal to the direction (x) of the prevailing wind whose speed is U. It is convenient to divide the temperature and pressure fields into mean background values $T_0(z)$ and $P_0(z)$ plus perturbations to these quantities induced by the plume. Let θ and p be the small perturbations to these quantities. Similarly, the gas density ρ_g is decomposed into an

ambient density ρ_0 and a small thermally induced perturbation. This perturbation is related to the temperature perturbation through the equation of state which is taken in the small disturbance, low Mach number form appropriate to this problem

$$\frac{\rho_g - \rho_o}{\rho_o} = -\frac{T - T_o}{T_o} \tag{13}$$

The ambient density is related to the background pressure through the hydrostatic balance

$$\frac{dP_o}{dz} = -\rho_o g \tag{14}$$

The background temperature is taken to be linearly stratified

$$T_o(z) = T_\infty\left(1 - \frac{z}{H}\right) \tag{15}$$

where T_∞ is the ground temperature and H is a length on the order of 30 kilometers. Over the first few kilometers in altitude, the background temperature changes by only a small fraction of its value at the ground. This together with equation (14) ensures that the fractional variation of absolute temperature and density are small if the plume calculation begins a few diameters of the fire downwind of the fire. Under these circumstances the equations governing the steady-state downwind evolution of the plume can be written in the Boussinesq approximation as follows

$$\frac{\partial v}{\partial y} + \frac{\partial w}{\partial z} = 0 \tag{16}$$

$$\rho_o\left(\frac{U\partial v}{\partial x} + \frac{v\partial v}{\partial y} + \frac{w\partial v}{\partial z}\right) + \frac{\partial p}{\partial y} = \mu\left(\frac{\partial^2 v}{\partial y^2} + \frac{\partial^2 v}{\partial z^2}\right) \tag{17}$$

$$\rho_o\left(\frac{U\partial w}{\partial x} + \frac{v\partial w}{\partial y} + \frac{w\partial w}{\partial z}\right) + \frac{\partial p}{\partial z} + (\rho - \rho_o)g = \mu\left(\frac{\partial^2 w}{\partial y^2} + \frac{\partial^2 w}{\partial z^2}\right) \tag{18}$$

$$\rho_o C_p\left(\frac{U\partial\theta}{\partial x} + \frac{v\partial\theta}{\partial y} + \frac{w\partial\theta}{\partial z}\right) - \left(\frac{dP_o}{dz} + \frac{\rho_o C_p T_\infty}{H}\right)w = k\left(\frac{\partial^2\theta}{\partial y^2} + \frac{\partial^2\theta}{\partial z^2}\right) \tag{19}$$

$$\frac{U\partial\rho_p}{\partial x}+\frac{v\partial\rho_p}{\partial y}+\frac{w\partial\rho_p}{\partial z}=0 \tag{20}$$

where ρ_0 is the ambient density, c_p the specific heat of air, k the thermal conductivity, and μ the dynamic viscosity. The prevailing wind speed in these equations U is taken to be constant and much larger than the crosswind velocity components. This second assumption is quite realistic several flame lengths downwind of the fire. Since U does not change, there is no need for a windward component of the momentum equations.

The quantities k and μ denote the effective eddy thermal conductivity and viscosity in the undisturbed atmosphere. It is used here as a means to represent the small scale mixing induced by the atmospheric turbulence. The eddy viscosity is dependent on the level of turbulence in the atmosphere, and is typically about three orders of magnitude larger than the true molecular viscosity of the air. Note that we are only using this concept to simulate the subgrid scale motions; i.e. motions on scales below the 5 -- 10 meter resolution of the calculations reported here. The large scale mixing processes are calculated directly. Even with the assumption of an eddy viscosity model for the small scale turbulence, the large eddy simulations performed require an ability to simulate flows at quite high Reynolds numbers.

The equations of motion must be supplemented with initial and boundary conditions. Since the details of the fire are not being simulated, the only quantities that are retained are the overall heat release rate Q and the particulate mass flux M. They are related to the local field variables through the integrals

$$\begin{aligned}\int_{-\infty}^{\infty}\int_{o}^{\infty}\rho_o C_p\theta U\,dz\,dy &= Q\\ \int_{-\infty}^{\infty}\int_{o}^{\infty}\rho_p U\,dz\,dy &= M\end{aligned} \tag{21}$$

The crosswind velocity components v and w are assumed to be zero initially. At the ground there is no vertical velocity, no plume induced heat transfer, and no wind shear. These assumptions are consistent with the assumed uniformity of the prevailing wind and the resolution limits of the calculation.

The far field conditions in the crosswind plane require that the perturbation temperature, perturbation pressure, and windward component of the vorticity vanish at the edge of the computational domain, which is drawn sufficiently far from the plume so as to minimize its effect on the computation.

We nondimensionalize the equations of motion so as to maximize the amount of information which can be extracted from each run. The independent and dependent variables are scaled as follows:

$$\theta = \frac{Q}{C_p T_\infty \rho_o U L^2}\hat{\theta} \qquad \rho_p = \frac{M}{\rho_o U L^2}\hat{\rho}_p$$

$$(y,z) = L(\hat{y},\hat{z}) \qquad (v,w) = V(\hat{v},\hat{w})$$

$$V = \left(\frac{Qg}{C_p T_\infty \rho_o U L}\right)^{\frac{1}{2}} \qquad x = \frac{UL}{V}\hat{t} \tag{22}$$

$$L = \left(\frac{QH}{C_p T_\infty \rho_o U \beta}\right)^{\frac{1}{3}} \qquad \beta = \frac{gH}{C_p T_\infty} - 1$$

$$Re = \rho_o VL/\mu \qquad Pr = \mu C_p/k$$

$$\alpha = \frac{Q}{MC_p T_\infty}$$

The dimensionless form of the conservation laws for the Large Eddy Simulation (LES) of a smoke plume trajectory are

$$\frac{\partial \hat{v}}{\partial \hat{y}} + \frac{\partial \hat{w}}{\partial \hat{z}} = 0$$

$$\frac{\partial \hat{v}}{\partial \hat{t}} + \hat{v}\frac{\partial \hat{v}}{\partial \hat{y}} + \hat{w}\frac{\partial \hat{v}}{\partial \hat{z}} + \frac{\partial \hat{p}}{\partial \hat{y}} = \frac{1}{Re}\left(\frac{\partial^2 \hat{v}}{\partial \hat{y}^2} + \frac{\partial^2 \hat{v}}{\partial \hat{z}^2}\right)$$

$$\frac{\partial \hat{w}}{\partial \hat{t}} + \hat{v}\frac{\partial \hat{w}}{\partial \hat{y}} + \hat{w}\frac{\partial \hat{w}}{\partial \hat{z}} + \frac{\partial \hat{p}}{\partial \hat{z}} + \frac{\hat{\rho}}{\alpha} - \hat{\theta} = \frac{1}{Re}\left(\frac{\partial^2 \hat{w}}{\partial \hat{y}^2} + \frac{\partial^2 \hat{w}}{\partial \hat{z}^2}\right) \tag{23}$$

$$\frac{\partial \hat{\theta}}{\partial \hat{t}} + \hat{v}\frac{\partial \hat{\theta}}{\partial \hat{y}} + \hat{w}\frac{\partial \hat{\theta}}{\partial \hat{z}} + \hat{w} = \frac{1}{PrRe}\left(\frac{\partial^2 \hat{\theta}}{\partial \hat{y}^2} + \frac{\partial^2 \hat{\theta}}{\partial \hat{z}^2}\right)$$

$$\frac{\partial \hat{\rho}_p}{\partial \hat{t}} + \hat{v}\frac{\partial \hat{\rho}_p}{\partial \hat{y}} + \hat{w}\frac{\partial \hat{\rho}_p}{\partial \hat{z}} = 0$$

with the associated boundary and initial conditions

$$\begin{aligned}
\hat{w} = \frac{\partial \hat{v}}{\partial \hat{z}} = \frac{\partial \hat{\theta}}{\partial \hat{z}} = 0 \quad \text{at } z = 0 \\
\frac{\partial \hat{w}}{\partial \hat{y}} - \frac{\partial \hat{v}}{\partial \hat{z}} = \hat{p} = \hat{\theta} = 0 \text{ as } \hat{y}, \hat{z} \to \infty \\
\iint \hat{\rho}_p(\hat{y}, \hat{Z}, 0)\, d\hat{y} d\hat{z} = \frac{1}{f^3} \\
\iint \hat{\theta}(\hat{y}, \hat{Z}, 0)\, d\hat{y} d\hat{z} = \frac{1}{f^3} \\
\hat{v}(\hat{y}, \hat{z}, 0) = \hat{w}(\hat{y}, \hat{z}, 0)\ 0
\end{aligned} \tag{24}$$

The magnitude of the initial temperature and density integrals is subject to a rescaling of certain variables meant to ensure that the plume remains within the computational domain. We denote the rescaled variables with an asterisk:

$$(\hat{y}, \hat{z}) = f(y^*, z^*),\ (\hat{v}, \hat{w}) = f(v^*, w^*),\ \hat{t} = t^*, \text{ and } \hat{\theta} = f\theta^*$$

To avoid confusion, we will write out the algorithm using the original notation, keeping in mind that the magnitude of the initial temperature and density profiles is subject to a rescaling.

The maximum height of the plume is very sensitive to the stability of the atmosphere as measured by the parameter β. Because the background temperature stratification given in equation (14) is subject to great uncertainty and difficult to determine empirically, it is possible to base the scalings on the actual observed plume height (if available) rather than upon any estimate of the value H. We derive the atmospheric scale height H from the scaling relations given above, writing H in terms of the plume height scale L

$$H = \frac{L^3 \rho_0 U c_p T_\infty}{L^3 \rho_0 U g - Q} \tag{25}$$

The height of the computational domain represents a physical height of fL, and this quantity may be calibrated from the observed plume height once a suitable value of f is chosen which ensures the plume remains within the boundaries of the computational domain.

It is relatively easy to prescribe a nonlinear temperature stratification. We define H in terms of some average temperature lapse rate

$$\frac{\overline{dT_0}}{dz} = -\frac{T_\infty}{H} \tag{26}$$

and the fourth of equations 23 is modified slightly

$$\frac{\partial\hat{\theta}}{\partial\hat{t}} + \hat{v}\frac{\partial\hat{\theta}}{\partial\hat{y}} + \hat{w}\frac{\partial\hat{\theta}}{\partial\hat{z}} + \frac{H}{\beta}\frac{1}{T_0}\left(\frac{dT_0}{dz} + \frac{g}{c_p}\right)\hat{w} = \frac{1}{PrRe}\left(\frac{\partial^2\hat{\theta}}{\partial\hat{y}^2} + \frac{\partial^2\hat{\theta}}{\partial\hat{z}^2}\right) \tag{27}$$

LES NUMERICAL METHOD

Equations (23) constitute a mixed system of partial differential equations; i.e., the equation for the temperature is parabolic, the equation for the particulate density is hyperbolic, and the equation for the pressure (which is derived from the incompressibility condition) is elliptic. The equations and the associated boundary conditions are solved using a relatively simple finite difference technique. The computational domain spanning the crosswind plane is one unit in the vertical direction and four units in the horizontal direction, representing a physical domain fL units high and $4fL$ units wide. This area is divided into rectangular cells (preferably square) with a uniform spacing in each direction. The horizontal velocity $\hat{v}$ is taken on the left and right boundaries of each cell, the vertical velocity $\hat{w}$ is taken at the top and bottom, and the perturbation temperature $\hat{\theta}$, pressure $\hat{p}$, and particulate density $\hat{\rho}_p$ are taken at cell centers. This placement of the flow variables leads to a very natural and efficient differencing scheme for the equations. We use central differences for all spatial derivatives and advance the solution in time (*i.e.* follow the evolution of the plume downwind) with a second order Runge-Kutta scheme. The equation governing the particulate density is solved in Lagrangian fashion by representing the particulate matter as particles of a certain mass which are advected with the flow. The pressure is found by applying the divergence-free condition to the momentum equations, yielding a Poisson equation. Due to the simple geometry of the problem this equation for the pressure may be solved using a very efficient fast solver.

LES RESULTS

We wish to compare a sample computation with data from the mesoscale burn 5/30 which is described in reference[13]. We scale our calculation as follows: Based on an observed plume height of approximately 800 meters, we determine the scale height L to be about 400 meters and the scaling factor f to be about 2.71. We determine the atmospheric scale height H from equation (25) to be about 32.5 km, given a heat loading Q=110 MW and a downstream velocity U=3 m/s. We use this value of H to calculate the characteristic crosswind velocity V as 1.55 m/s. The computational domain is divided into a rectangular grid 192 cells high and 768 cells wide for the calculation described here. The resolution of the computational grid determines the maximum resolvable Reynolds number for a given run. Roughly, this maximum value scales as the square of the number of grid cells in the direction of the domain height. With the grid of 768 × 192 cells, we have used a Reynolds number of 20,000 and a Prandtl number of 1.

Figure 20 compares the "centerline" plume trajectory with the observed data. Based on the observed plume trajectory reported in Table 18 of reference [13], we prescribe an initial circular plume cross section 210 meters downwind of the fire with a radius of 65 meters and centered approximately 80 meters off the ground. Figures 21 and 22 show the development of the plume in the first few thousand meters downwind of the source. Of particular interest in these figures are the two main vortices which entrain a large amount of the particulate and surrounding air. The ambient stratification introduces a natural frequency into the problem which results in a damped oscillation of the plume about the level of neutral buoyancy as its contents mix and disperse. In Figures 21 and 22, the vortices can be seen separating, deflecting off the level of neutral buoyancy, and then reuniting.

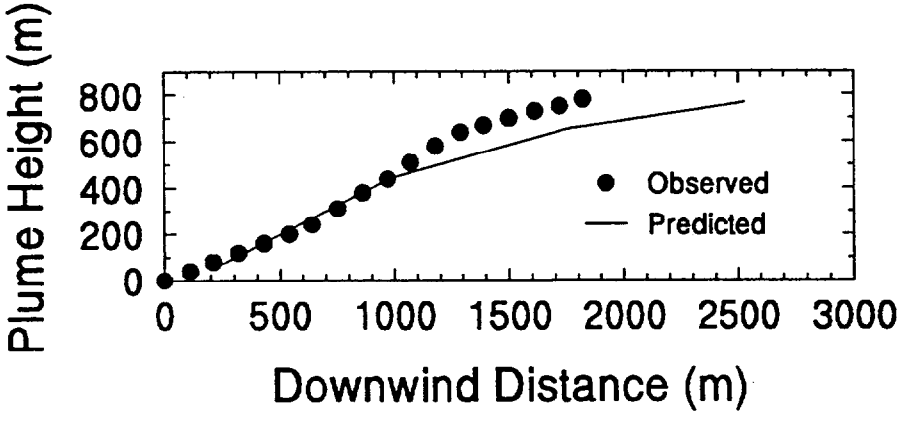

Figure 20. Centerline plume height for mesoscale crude oil burn 5/30

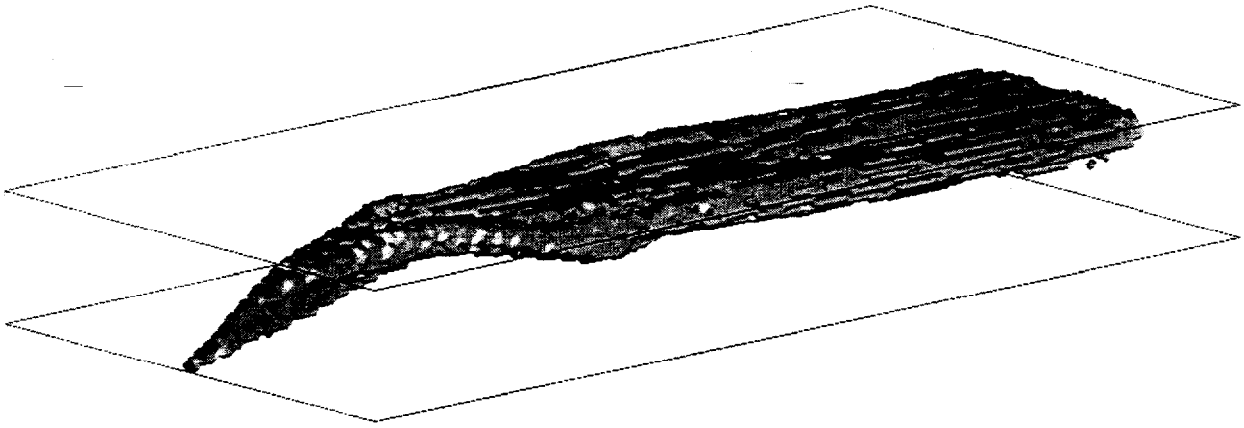

Figure 21. Three dimensional view of the windswept plume. Shown is the particulate matter, whose initial profile is located 210 m downwind of the fire. The viewing area is 1,100 m high, 4,400 m wide, and 8,800 m long (windward direction). The particles are convected downwind at a speed of 3 m/s.

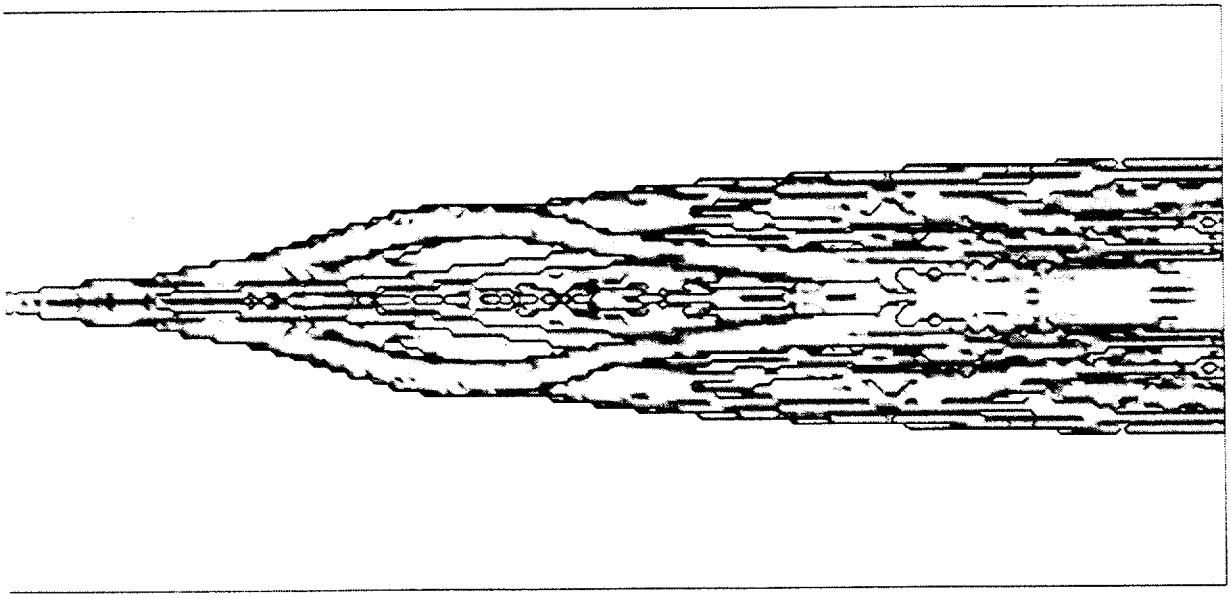

Figure 22. A view of the plume from below. Note the separation and reconnection of the two major vortices

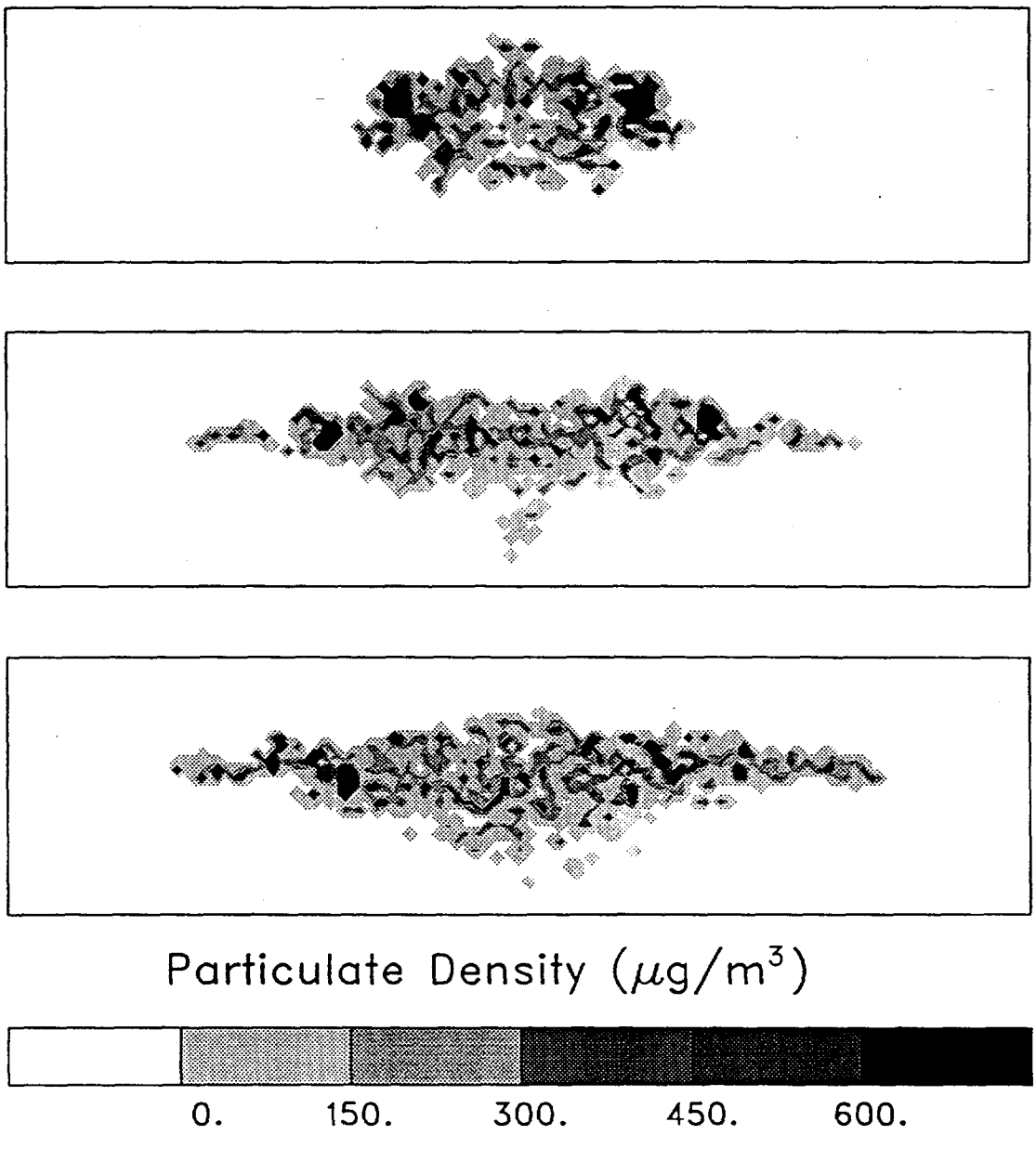

Figure 23. The particulate distribution further downwind. The height of the viewing area is approximately 1,100 m. The first profile is 8 km downwind of the fire, the second profile is 15 km downwind, and the third is 23 km downwind. The particles are convected downwind at a speed of 3 m/s.

Downstream of the fire, the particulate matter will, in general, rise with the heated plume and later descend after the plume has cooled. Since the combustion products and the particulate matter will produce a cooled plume only slightly more dense than the surrounding air, the descent of the plume will be rather slow compared to its rise. Figure 23 shows cross sections of the plume tens of kilometers downwind. Notice that the large scale mixing and diffusion have scattered the particulate evenly throughout the plume cross section. This particulate profile may persist for hundreds of kilometers depending on the ratio of thermal to combustion-product-mass buoyancy loading (denoted by the parameter α). Although not calculated directly this shape is similar to that observed in figure 19. Information of this type is of great interest in populated areas, where the distance from the source that combustion products remain aloft is very important. It is possible to analyze the particulate density field to determine where certain concentrations of particulate density will be found, and how far downwind one might expect to find such levels. This type of analysis is very useful in determining where the plume might pose a health problem, especially in cases of concern where the plume does not rise far from the ground.

It is possible to extend the simulation into the third section of the plume trajectory described in the introduction, which covers length scales on the order of hundreds of kilometers downwind. We caution, however, that in this range meteorological conditions dominate the motion of the particulate matter, which by this point has lost all vestiges of the original fire. Figure 24 shows the footprint of the particulate over about 150 kilometers. In the absence of crosswinds and other statistical fluctuations induced by the prevailing meteorological conditions, the model predicts that the particulate will fall within an extremely narrow path. In reality, this is obviously not the case, but rather can be thought of as a "worst case" scenario relative to concentrations and the best case relative to the crosswind area effected.

The model of plume dispersion presented above is best described as a deterministic model valid in an intermediate region downstream from the fire source. Within a few fire diameters of the source, the heat release is intense and the Boussinesq approximation is not valid. Also, the approximations which allow replacement of a three-dimensional steady plume by a two-dimensional time dependent one are not valid near the fire because the buoyant velocity of the plume is comparable to the cross wind. Therefore, the plume is being "bent over" in this region, and a fully three-dimensional and time dependent model of the plume rise in a cross flow must be developed to adequately describe this region near the fire source. Similarly, the meteorological assumptions of the model become increasingly questionable further downstream. One of these is the assumption of a steady uniform wind blowing over the fire; variations in both wind speed and direction must affect results the longer in time (or further downstream) one runs the calculation. Another assumption is that of a purely deterministic model; variations in meteorological conditions, including wind speed, direction, and atmospheric turbulence level, all imply that statistical variations will become more dominant at greater distances from the fire source. For this deterministic model, no account has been taken of such statistical variation. For these reasons, there is an intermediate region, not too close to the source, but, then again, not too far downstream, for which this model has predictive capability, and this region

depends upon the fire and meteorological conditions. For the case examined, it is estimated that predictions are applicable in the region between 200 m and 20-30 km from the fire source.

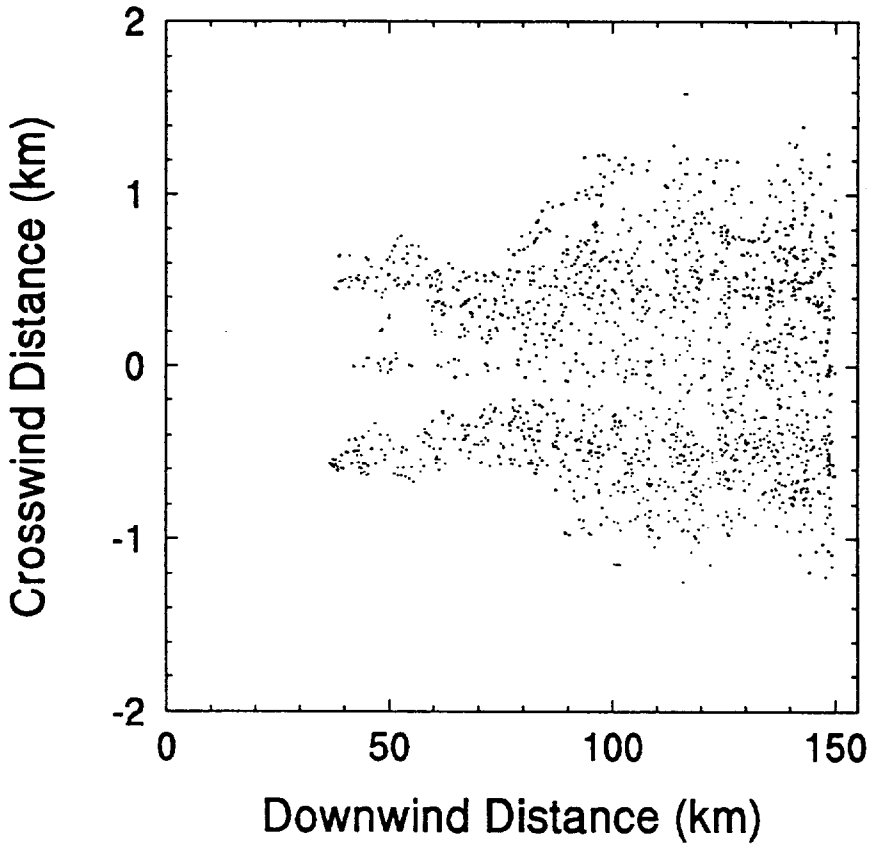

Figure 24. The footprint of the particulate deposition far downwind. Note the difference in crosswind and windward length scales

CONCLUSIONS

In the mesoscale experiments, the wind speed did not appear to affect the average burning rate but did contribute to variations in burning extinction. The recommended value to use for the burning rate of large thick layers of fresh Louisiana crude oils on water is 0.052 ± 0.002 kg/s/m^2 (5.4 ± 0.2 gal/hr/ft^2).

It was generally found that well over 90 percent of the fresh oil was consumed in the pan burns. In addition, the residue from the primary burn could be corralled and burned with the addition of kerosene as an ignitor.

Although smoke yield depends on fire diameter, the smoke yield from the 17.2 m effective diameter mesoscale fire was the same as that for the 1.2 m diameter large laboratory pan burn at FRI. Measurements from the mesoscale experiments are more scattered than the laboratory measurements, but the smoke yield value of 11 ± 1% represents most of these measurements for fresh Louisiana crude oil. Moreover the laboratory measurements indicated that the smoke yield was essentially independent of radial position within the plume.

The size distributions of aerodynamic effective diameters for the smoke particulate were nearly identical for the 1.2 m diameter laboratory fire and a 17.2 m effective diameter mesoscale fire. This indicates the results of a 1.2 m diameter burn could be used directly to predict the size distribution of larger diameter burns. Most of the particulate mass was below 10 μm in diameter as measured with a cascade impactor.

ACKNOWLEDGEMENTS

This work was funded by the Technology Assessment and Research Program for Offshore Minerals Operations, Minerals Management Service, U.S. Department of the Interior, managed by John Gregory and Ed Tennyson.

The cooperation and support of the U.S. Coast Guard Research and Development Center made the use of the mesoscale burn site possible. The Environmental Safety Branch, under the direction of Commander Pete Tebeau provided funding for operation of the mesoscale test site and Dave Beene of the Marine Fire and Safety Research Branch and the Fire and Safety Test Detachment in Mobile provided outstanding assistance in preparing for and conducting the mesoscale burn experiments.

We would like to thank Kunihiro Yamashita, chief of the First Division for support of the experiments at FRI in Japan.

Donation of crude oil for the experiments was made by the Marine Industry Group (MIRG) through Ron Benton of Shell Oil Company, chairman (MIRG) and the Marine Spill Response Corporation (MSRC) through Jim Simmons provided for the transportation of the crude oil from Louisiana to Mobile and the deliveries to the mesoscale burn site.

J. Randall Lawson, Jay McElroy, Roy McLane and Robert Vettori of the Building and Fire Research Laboratory, NIST provided immeasurable assistance in conducting the mesoscale burns.

Appreciation is extended to the U.S. Coast Guard Aviation Training Center for providing a helicopter and crew which made aerial observations of the plume possible.

REFERENCES

1. Smith, N.K. and Diaz, A., In-place burning of Prudhoe Bay Oil in broken ice. Proceedings 1985 Oil Spill Conference, Prevention, Behavior, Control, Cleanup. pp. 405-410, 1985.

2. Tennyson, E.J., Results from Selected Oil Spill Response Research by the Minerals Management Service - Marine Technology Society Journal Volume 24 Number 4, pp 27-32, 1990

3. Brown, H.M. and Goodman, R.H., "In Situ Burning of Oil in Ice Leads," Proceedings of the Ninth Annual Arctic and Marine Oilspill Program Technical Seminar, June 10-12, 1986, Edmonton, Alberta, Canada, Environment Canada, Ottawa K1A 0H3, pp. 245-256, 1986.

4. Buist, I.A., and Twardus, E.M., "Burning Unconfined Oil Slicks: Large Scale Tests and Modelling," Proceedings of the Eighth Annual Arctic Marine Oilspill Program Technical Seminar, June 18-20, 1985, Edmonton, Alberta, Canada, Environment Canada, Ottawa K1A 0H3, pp. 103-130, 1985.

5. Evans, D., Baum, H., McCaffrey, B., Mulholland, G., Harkleroad, M., and Manders, W., "Combustion of Oil on Water," Proceedings of the Ninth Arctic Marine Oilspill Program Technical Seminar, June 10-12, 1986, Edmonton, Alberta, Ministry of Supply and Services Canada Cat. No. En 40-11/5-1986E, pp. 301-336, 1986.

6. Evans, D., Mulholland, G., Gross, D., Baum, H., and Saito, K., "Environmental Effects of Oil Spill Combustion," Proceedings of the Tenth Arctic and Marine Oilspill Program Technical Seminar, June 9-11, 1987, Edmonton, Alberta, Ministry of Supply and Services Canada Cat. No. En 40-11/5-1987E, pp. 91-130, 1987.

7. Evans, D., Mulholland, G., Gross, D., Baum, H., and Saito, K., "Burning, Smoke Production, and Smoke Dispersion from Oil Spill Combustion," Proceedings of the Eleventh Arctic and Marine Oil Spill Program Technical Seminar, June 7-9, 1988, Vancouver, British Columbia, Ministry of Supply and Services Canada, Cat. No. En 49-11/5-1988 E/F, pp. 41-87, 1988.

8. Evans, D., Baum, H., Mulholland, G., Bryner, N., and Forney, G., "Smoke Plumes From Crude Oil Burns," Proceedings of the Twelfth Arctic and Marine Oil Spill Program Technical Seminar, June 7-9, 1989, Calgary, Alberta, Ministry of Supply and Services Canada, Cat. No. En 40-11/5-1989, pp. 1-22, 1989.

9. Evans, D., Walton, W., Baum, H., Lawson, R., Rehm, R., Harris, R., Ghoniem, A., Holland, J., "Measurement of Large Scale Oil Spill Burns," Proceedings of the Thirteenth Arctic and Marine Oil Spill Program Technical Seminar, June 6-8, 1990, Edmonton, Alberta, Ministry of Supply and Services Canada, Cat. No. En 40-11/5-1990. pp. 1-38, 1990.

10. Benner, B. A. Jr., Bryner, N. P., Wise, S. A., Mulholland, G. W., Lao, R. C., Fingas, M. F., "Polycyclic Aromatic Hydrocarbon Emissions from the Combustion of Crude Oil on Water," Environmental Sciences & Technology, Vol. 24, pp. 1418-1427, 1990.

11. Evans, D., Walton, W., Baum, H., Mulholland, G., Lawson, J., Koseki, H., Ghoniem, "Smoke Emission from Burning Crude Oil," Proceedings of the Fourteenth Arctic and Marine Oil Spill Program Technical Seminar, June 12-14, 1991, Vancouver, British Columbia, Ministry of Supply and Services Canada, Cat. No. En 40-11/5-1991. pp. 421-449, 1991.

12. Evans, D., Tennyson, E.J., In-Situ Burning -- A Promising Oil Spill Response Strategy, Seventh Symposium on Coastal and Ocean Management, July 8-12, 1991, Long Beach, California, conference preprint, 1991.

13. Evans, D., Walton, W., Baum, H., Notarianni, K., Lawson, J., Tang, H., Keydel, K., Rehm, R., Madrzykowski, D., Zile, R., Koseki, H., and Tennyson E., "In-Situ Burning of Oil Spills: Mesoscale Experiments," Proceedings of the Fifteenth Arctic and Marine Oil Spill Program Technical Seminar, June 10-12, 1992, Edmonton, Alberta, Ministry of Supply and Services Canada, Cat. No. En 40-11/5-1992. pp. 593-657, 1992.

14. Hering, S.V. (editor), Air Sampling Instruments for Evaluation of Atmospheric Contaminates, 7th Edition, American Conference of Governmental Industrial Hygienists, Cincinnati, Ohio, 1989.

15. Marple Personnel Cascade Impactors, Series 290, Instrument Manual, Bulletin No. 290I.M.-3-82, Sierra Instruments, Inc, Carmel Valley, CA.

16. Walton, W., "In Situ Burning of Oil Spills: Mesoscale Experiments," National Institute of Standards and Technology, Gaithersburg, MD, NISTIR, to be published.

17. United States Environmental Protection Agency, 40 CFR 60, 1992.

18. Tomany, James P. Air Pollution: the Emissions, the Regulations, & the Controls. Elsevier, New York, NY, 1975.

19. Voigt, H., Avlund, M., "Standardized Smoke." Elektronikcentralen, Danish Research Centre for Applied Electronics, Hørsholm, Denmark, June, 1980.

20. Drysdale, D. An Introduction to Fire Dynamics. John Wiley and Sons, New York, NY, 1985.

21. Leonard, J., Budnick, E., Back, G., Ganey, S., "Development of a Video Image-Based Methodology for Estimating Large Scale Transient Hydrocarbon Smoke Plume Size and Extent." National Institute of Standards and Technology, Gaithersburg, MD, NIST-GCR-92-614, August, 1992.

22. Hoshizaki, H., Wood, A., Seidenstien, S., Brandalise, B., Meyer, J., "Development of an Analytical Correlation Between Gas Turbine Engine Smoke Production and Jet Plume Visibility." Lockheed Palo Alto Research Laboratory, Palo Alto, CA, AFAPL-TR-76-29, January, 1976.

23. Humphreys, W.J., Ways of the Weather. Jaques Cattell Press, Lancaster, PA, 1942.